DESIGN OF A DETACHABLE ACOUSTICALLY-ACTUATED PLATFORM FOR SEPARATION OF WHOLE BLOOD AND NANOPARTICLES

A Thesis

by

ANNA MARIE WISNIOWIECKI

Submitted to the Office of Graduate and Professional Studies of
Texas A&M University
in partial fulfillment of the requirements for the degree of

MASTER OF SCIENCE

Chair of Committee,	Gerard L. Coté
Committee Members,	Jun Kameoka
	Brian E. Applegate
Head of Department,	Michael J. McShane

December 2018

Major Subject: Biomedical Engineering

ABSTRACT

Blood-based diagnostic tests have become a widespread paradigm for clinical disease diagnosis. Such tests are designed to detect small molecules in blood, which are indicative of a particular disease. Current blood-based diagnostic tests utilize specialized equipment, manual steps, and trained technicians. These factors limit the access of patients to testing. Lab-on-a-chip techniques, which enable handling of samples on the micron scale, have the potential to replace and simplify the current processes. In addition, sensitive optical assays that utilize functionalized nanoparticles have been developed for applications at the point-of-care. These assays require a consistent nanoparticle concentration. In this work, an acoustic platform to replace the first step in blood-based diagnostic assays, blood separation, is developed and tested for use with nanoparticle-based assays.

The presented system uses a surface acoustic wave transducer integrated with a detachable microfluidic channel to achieve blood separation. The concept of a single-injection system, in which nanoparticles are mixed with an unprocessed sample, is tested. A standing wave generated by the transducer creates areas of high and low pressure across the microfluidic channel that cause displacement of blood components, based on size, from the sample stream to adjacent buffer fluid streams. The ability of this system to separate undiluted whole blood and nanoparticles is assessed. Fabrication of the standing surface acoustic wave transducer and microfluidic channel are described in detail. A detachable system is proposed to allow reuse of the transducer. Results from blood separation experiments using different transducer and channel designs are presented. To improve the transducer performance in experiments longer than several minutes, a temperature-regulation system was built. The first whole blood separation experiment

using a detachable microchannel and standing surface acoustic waves is reported. Finally, the effect of the acoustic mechanism on functionalized nanoparticles is tested. The results indicate that a detachable acousto-fluidic system using surface acoustic waves may be used for effective whole blood separation when using temperature regulation. For maintenance of nanoparticle concentration and use of a single-injection system, the acoustic properties of the buffer must be tuned.

ACKNOWLEDGEMENTS

I would like to thank my committee chair, Dr. Gerard L. Coté, for his guidance, advice and support throughout this research. I would also like to thank my committee members, Dr. Jun Kameoka and Dr. Brian Applegate, for their advice and support. In addition, I greatly appreciate the generosity of Dr. Jun Kameoka, as well as Dr. Abhishek Jain, Dr. Mary McDougall and Dr. Stephen Wright, in giving me access to their labs and expertise.

Thanks also go to my friends and colleagues, including Travis Carrell, Matthew Wilcox, Romina del Bosque, David Luna, Navaneeth Krishna, Serge Dogbevi, Andrea Locke, Javier Garza, Sina Baghbani Kordmahale, Jaskirat Batra, Po-Jung Huang, Cody Lewis, Richard Horner, Lee Hudson, Dandan Tu, Lydia Colvin and Samantha Holt, who lent their ears and shared their expertise. This project could not have been done without you.

Finally, thanks to my mother, father, brother and grandmother for their encouragement and support.

CONTRIBUTORS AND FUNDING SOURCES

Contributors

This work was supported by a dissertation committee consisting of Professor Gerard L. Coté and Professor Brian E. Applegate of the Department of Biomedical Engineering and Professor Jun Kameoka of the Department of Electrical Engineering. The surface acoustic wave transducers were fabricated in collaboration with Sina Baghbani Kordmahale. The LabVIEW code for controlling the temperature regulation system was written in collaboration with Cody Lewis. All other work conducted for the thesis was completed by the student independently.

Funding Sources

Graduate study was supported by the Office of Graduate and Professional Studies Diversity Fellowship from Texas A&M University.

NOMENCLATURE

BAW	Bulk Acoustic Wave
IDT	Inter-digitated Transducer
IPA	Isopropyl Alcohol
LOC	Lab-on-a-Chip
PBS	Phosphate-Buffered Saline
PDMS	Polydimethylsiloxane
POC	Point-of-Care
SAW	Surface Acoustic Wave
SSAW	Standing Surface Acoustic Wave
TSAW	Traveling Surface Acoustic Wave
UV	Ultraviolet

TABLE OF CONTENTS

Page

LIST OF FIGURES

Page

Page

Page

Page

LIST OF TABLES

Page

CHAPTER I

INTRODUCTION AND BACKGROUND

1.1 Introduction

Blood-based diagnostic tests have become a widespread paradigm for clinical disease diagnosis. Such tests are designed to detect small molecules ("biomarkers") in blood, which are indicative of a specific disease. Current blood-based diagnostic tests are carried out in centralized laboratories within hospitals or through external lab services. Tests typically use centrifuges for blood separation and other bulky, specialized analysis tools. Current processing times and subsequent delivery of test results effect the time to treatment. Delivering results to patients can take hours to days (1, 2). Additionally, trained technicians are required to perform manual steps and analyze results (3, 4). By reducing or eliminating these requirements, diagnostic tests would be accessible to new patient populations, while enabling faster, lower cost, and more accessible diagnoses for patients where resources are already available. These factors limit the access of the patient to treatment, specifically limiting the use of diagnostic testing in the field (such as in small towns or on the battlefield), by the bedside (in the emergency room, home, etc.) and in other low-resource environments. An automated platform implemented at the patient's side, in addition to increasing the ability to diagnose, would reduce the instance of erroneous results and reduce timeframes, leading to earlier treatment. Such a platform would be particularly impactful for patient populations in remote regions, lacking a physician or health center, who must travel to get care and during emergency situations, where point-of-care (POC) results are needed to guide treatment. There is a need to develop technology to enable POC diagnostics. The ideal,

"accessible" diagnostic platform would be portable, single-step, fast, low-cost, sensitive, specific, and reduce the need for trained technicians.

A group of technologies termed lab-on-a-chip (LOC) technologies, spanning advances in micron- and nanometer-scale fabrication and manipulation, has been proposed to provide all components of a process in a small, portable and simple format for applications including biological and environment monitoring (4-6). Microfluidic technology, for instance, which enables handling of samples on the micron scale, is one example of a LOC technology and one of the most widely accepted prospects for diagnostic platforms (7). The technology requires only small sample volumes and offers a length-scale comparable to cells and biomarkers of interest, facilitating its potential to provide precise control of a sample. LOC technologies are uniquely poised to perform sample processing and have already been implemented in combination with other LOC technologies to address limitations of current diagnostics. Many blood-based diagnostic tests require sample preparation to remove interfering molecules, especially large blood cells, and to enable sensitive detection of biomarkers (8-10). Biomarker concentrations may be very low; for instance, cardiac troponin I, used for diagnosis of myocardial infarction, is found in concentrations of ng/L (11). Therefore, it is important that sample preparation and other operations do not alter the concentration of the biomarker. As blood filtration is an essential step for most diagnostic tests, new methods that improve this process can positively impact the development of accessible diagnostic tests, which is of great interest.

Due to the compatible length scales of microfluidics with acoustic wavelengths and also with biological cells, acoustic separation of biological samples has been explored and shown promising results toward diagnostic and clinical cell filtration or separation and toward addressing limitations of current and other proposed techniques (10, 12). In addition, sensitive

optical assays that utilize functionalized nanoparticles for applications at the POC are being developed by many groups (13, 14). By combining acoustic methods and advances in LOC technologies with these highly specific assays, there is potential to develop an accessible platform for diagnostic tests. While much progress has been made, the potential of LOC technology for translation and for POC diagnostic tests has not been proven (3, 4). A primary goal of the work proposed here is to assess the feasibility of an acoustic, microfluidic (or acousto-fluidic) platform for blood separation and functionalized nanoparticle-based assays as a basis for a POC diagnostic test. In particular, a reusable transducer and disposable microfluidic are developed and integrated, and the ability of the system to separate blood cells from plasma and recover nanoparticle assay components is evaluated.

1.2 Acoustic Blood Separation

Multiple mechanisms for blood filtration in LOC/POC format have been developed. Each of these methods has advantages for specific applications (7, 15). Methods include inertial, centrifugal, size exclusion, dielectrophoresis, magnetophoresis, acoustophoresis, and others methods such as using physical structures for cell separation. These techniques have achieved high separation efficiencies (up to 99% removal of cells) but also suffer from disadvantages. Inertial methods require sample dilution and suffer from low efficiency. Centrifugal methods have proved difficult to scale down. While dielectrophoresis achieves high efficiency, the risk of cell damage, hydrolysis and thermal convection may also be high. Magnetophoresis also suffers from harmful biological effects and often requires samples with innate magnetic properties (such as hemoglobin) or addition of magnetic tags to particles in the sample. Physical arrays and size exclusion methods tend to clog when using cell-dense samples such as blood. Miniaturization and ease of manufacturing are other issues common issues with existing techniques.

Acoustic-based blood separation provides a flexible mechanism for sample handling (12). In acoustophoretic blood separation, pressure waves, with wavelength comparable to blood components, are coupled into a microfluidic channel which contains the sample. As the sample is pumped through the channel, acoustic forces are exerted on blood components based on their mechanical properties, primarily size, to create sorting. High selectivity of sorted particles may be achieved by selection of the wavelength and transducer design. While acoustic mechanisms also face challenges in miniaturization and with low flow rates and heating, acoustic methods have achieved similar separation performance to the previously mentioned methods and enable generation of multiple forces, which can be tuned for particular operations (sorting, mixing, centrifugation, jetting, etc.) and applications. Acoustophoresis is gentle, label-free and contact-free. In particular, this method has the capability to handle undiluted whole blood (16). In addition, acoustic platforms are easy to manufacture by standard and commercial techniques. Potential disadvantages of acoustophoresis for LOC and POC applications are low throughput (low flow rates) and use of power. Increasing throughput of these systems is a topic of current research (29). Use of power is acceptable for some LOC and POC applications, such as at the bedside in a clinic or ambulance; however, for some lower resource environments, power requirement may limit the implementation of the technology. Based on the selectivity, flexibility, and other advantages of acoustic methods compared with other methods, an acoustic technique was selected for its potential for POC applications.

1.2.1 Theory

Acoustic manipulation takes advantage of the inverse piezoelectric effect to generate pressure waves. The piezoelectric effect is a property displayed by piezoelectric materials. These materials generate electric voltage upon being stressed or strained. This behavior is reversible,

with applied AC voltage creating mechanical force. Acoustic manipulation uses this inverse phenomenon to control position and motion of a sample for applications such as environmental, food safety, biological monitoring and sample handling.

Acoustic forces offer mechanisms for differentiating and actuating sample components. When pressure waves are injected into a system with increased magnitude from conventional imaging ultrasound and the particle radius is less than the acoustic wavelength ($r<<\lambda_{acoustic}$), the scattering of pressure waves may create a force of magnitude large enough to move particles or cells (17). Practically, the force seen by the particles is only significant when the particle diameter approaches the acoustic wavelength, lending it to the manipulation of micron-sized particles and cells with size which are compatible with commonly available acoustic frequencies (kHz - MHz). The force generated on the particle can be described as created by Mie scattering of the acoustic wave resulting in anisotropic-dominated scattering; for smaller particles, scattering transitions from the Mie regime to Rayleigh scattering regime resulting in a less directional force (18). The force generated is non-zero when time-averaged over the acoustic period (19). This force is referred to as acoustic radiation force (ARF) and scales with r^3, where r is particle radius, offering a size dependent separation mechanism. In addition, the acoustic radiation force (ARF) magnitude depends on density and compressibility of the particles and suspending medium (20). The equation for ARF is given by (16),

$$F_r = -(\frac{\pi p_0 V_p \beta_m}{2\lambda})\phi(\beta,\rho)\sin kx$$

$$\phi = \frac{5\rho_p - 2\rho_l}{2\rho_p + \rho_l} - \frac{\beta_p}{\beta_l}$$

Where F_r, p_0, V_p, β_m, λ, β, ρ, k and x are the acoustic force, pressure amplitude, particle volume, compressibility of the suspending medium, wavelength, compressibility, density, wave

number, and distance from node to anti-node. Φ is called the acoustic contrast factor, which describes the direction of the force on a particle. For a standing wave, a positive or negative value of the acoustic contrast factor indicates whether a particle will move towards the zero pressure or maximal pressure nodes (node and anti-node, respectively). Subscripts p and l refer to the properties of the particle and its suspending liquid. As can be seen, the size of the particle has a greater impact on the magnitude of the force seen by the particle, as compared with compressibility and density. Separation of particles by density and compressibility have been successful for particular applications where a significant difference in properties exists (21). However, size-based particle and biological cell separation have dominated successful applications of the technology (21, 22), including blood and cancer cell sorting.

Secondary forces, primarily acoustic streaming, have also been utilized particularly for micro-mixing and acoustic-driven centrifugation but also in the emerging field of nano-scale particle manipulation (12, 18). Acoustic streaming occurs where the wave enters the fluid. Acoustic streaming force (ASF) is derived from the nonlinear terms in the Navier-Stokes equation and manifests as body forces exerted on the fluid which results in steady fluid motion. It is the time-averaged viscous motion of the bulk fluid caused by absorption of energy and often manifests as a lateral recirculation of the suspending fluid (19). The Stokes (or viscous) drag force arises from the acoustic streaming force in the opposite direction from the ARF. Stokes drag force on particles scales with r and, subsequently, the overall radiation force on particles scales with r^2 (20). The equation for Stokes drag force is given by (23),

$$F_v = 6\pi\eta r v$$

Where η is fluid viscosity, r is particle radius, and ν is relative velocity between the particles and medium. While microfluidics are highly laminar systems, acoustic streaming may

be used as the dominate force by introducing asymmetry to the acoustic path. ASF exists at low magnitude for large cells in systems where the frequency is selected to primarily generate ARF on the large cells but increase when using higher frequencies (18). Bjerknes force is another secondary force present and applied in some applications (19). Bjerknes force is an inter-particle force generated by scattering from oscillating particles. The attractive Bjerknes force has been used for particle trapping. The secondary forces dominate behavior in the regime of relatively small biomarkers and nanoparticles, which experience ARF at magnitudes too low to overcome surface and viscous forces (18).

Using a single acoustic generator, the primary ARF manifests as a net unidirectional force, unless a reflector is placed at a distance $n(\lambda/2)$, where n is any integer. If two acoustic transducers are used and placed at a distance $n(\lambda/2)$ from one another, or one transducer and a reflector, a standing wave using the ARF can be created and used for particle manipulation. Standing waves have emerged as the preferred implementation of acoustophoresis for biological cell manipulation (24). Forces exerted using standing waves are higher for a given frequency and power (12). A standing surface wave system creates an interference pattern. Areas of high and low pressure develop along the cross-section of a sample and exert acoustic radiation forces that attract particles to the maximum and minimum nodes based on acoustic contrast. This pressure distribution creates a 2D sorting scenario. For instance, for a blood sample, the acoustic contrast factors are positive for platelets, red blood cells and white blood cells (16), causing all of the components to migrate toward the node at rates based on the ARF magnitude for that particle type. Micron dimension channels have commonly been used to contain the particles and perform manipulation. By dimensioning the channel, drift of particle types due to the ARF can be used to separate the sample. Fig. 1 illustrates a standing wave setup using two types of acoustic

transducers, which are discussed further below: bulk acoustic wave (BAW) transducers, and surface acoustic wave (SAW) transducers.

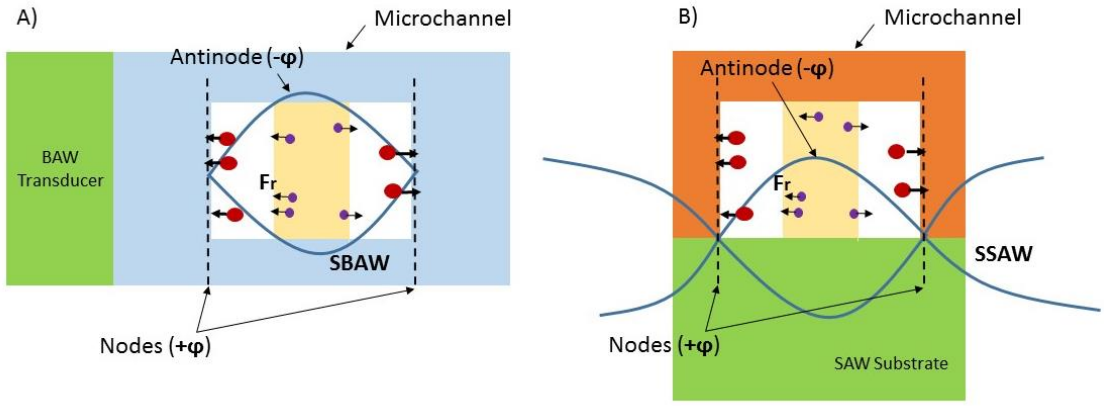

Fig. 1 Standing wave setup for microfluidic sorting of blood cells using acoustophoresis. Two types of acoustic transducer are primarily used for cell sorting experiments: A) bulk acoustic wave (BAW) transducers and B) surface acoustic wave (SAW) transducers. Using a BAW transducer, the channel is used to form the standing wave by using acoustically reflective materials. Using a SAW transducer, multiple electrodes create a standing wave between them and the channel is aligned to achieve nodal placement. For cell sorting experiments, the sample is often placed in the center stream for efficient sorting and nodes are placed near the channel walls. When the transducer is turned on, standing waves are formed (SBAW or SSAW) and acoustic radiation force (F_r) is exerted on blood components based on size. As all blood components have positive acoustic contrast, all components are driven toward the nodes. Large cells experience the greatest force and arrive at the nodes first.

1.2.2 Bulk Acoustic Waves (BAW) for Acousto-fluidic Blood Separation

Two varieties of acoustic transducers have been explored for particle manipulation and microfluidic operations: conventional bulk acoustic wave transducers, which transmit pressure waves throughout the bulk of the transducer and into the sample, and surface acoustic wave transducers, which generate a traveling wave on the surface of the piezoelectric substrate via resonant electrodes. Bulk wave transducers are low cost, but typically generate lower frequencies, less than 10 MHz, due to the efficiency of the manufacturing process. Lower frequencies are more likely to generate harmful effects on cells (12). Higher frequencies, in the MHz range, enable finer manipulation as well as reducing the likelihood of harmful biological effects. In addition, bulk transducers require sample cells with high acoustic transmission properties, such as etched silicon or glass microchannels. These (usually) layered devices suffer from energy loss (heating) in the transducer and require precision mounting to ensure proper acoustic transmission. In many BAW cell sorting platforms, the microfluidic device is involved in standing wave formation, which also requires precise mounting. Bonding methods to the sample cell are generally permanent. POC applications require lower cost solutions, such as a disposable sample cell and reusable transducer.

Studies manipulating blood with BAW transducers have achieved separation efficiencies greater than 99% (10, 25) and attempted to mitigate the limitations of prior systems. In 2009, Lenshof et al. separated plasma from whole blood using a silicon and glass channel with ultrasound gel coupling to a 2 MHz BAW transducer (26). The design used a winding channel with multiple outlets for removing blood cells, avoiding over-crowding at nodal positions. While this study used gel-coupling, precise mounting was still necessary for the transducer used. 12.5% clean plasma was extracted, with purity meeting regulatory standards for diagnostic quality;

however, the study targeted isolating prostate specific antigen in plasma and a significant amount of biomarker loss was observed. Since then, this system has been improved by incorporating a sheath fluid through a tri-furcated channel design, impedance-matching the sheath fluid and adding a temperature-regulation system (10, 27-29). Several fluids have been used to reduce the problem of density mismatch between suspension fluids, enabling an increase in sample cell concentration from 1 to 20% while maintaining separation of >99% and high recovery of bacteria and cancer cells needed for diagnostics, as well as increasing throughput. Much of this work in development of BAW for cell sorting has come from Thomas Laurell's group. In the last few years, the group published an integrated study, combining their blood separation chip with an acoustic trapping capillary and a polymerase chain reaction chip for sepsis diagnostics. The chip was proposed for rapid sepsis diagnostics and measured clinically-relevant levels of bacteria. Stationary sample cells for blood analysis of plasma using SSAW have also been proposed (30), but limit the performance of additional processes on the sample and present potential for noise during detection.

Similar application in cell concentration have produced additional interesting designs. A design for a single inlet channel was proposed to separate circulating tumor cells from white blood cells, cells of similar size, using a two stage separation system (31). A 4.5 MHz transducer was first used to pre-align the sample and a 2 MHz transducer was used in the following region to isolate tumor cells with 95-100% separation efficiency. The sample was diluted but the system provided improved throughput above previous designs. Another study used a recirculating channel to concentrate circulating tumor cells from dilute solutions (32).

Due to the low flow rates required by acoustophoresis, high-throughput designs have also been an area of research. Using impedance-matched buffer fluid, a BAW blood separation

experiment achieved a throughput of 1 mL in 25 minutes removing 99.8% of blood cells (27). Several custom BAW systems have been built to address throughput limitations. A syringe with a brass case and multiple 4.5 MHz BAW transducers was built for the generation of autologous platelet-rich plasma (33). The design achieved improved platelet concentration and purity. In another design, a custom, aluminum channel was machined and coupled to a BAW transducer for separation of whole blood (29). The channel has upper and lower flow streams allowing for removal of blood cells and processed 10 mL/min with 80% removal of large cells.

1.2.3 Surface Acoustic Waves (SAW) for Acoustofluidic Blood Separation

Surface acoustic wave (SAW) transducers offer a viable solution for cell manipulation, which approaches POC requirements. SAW technology has been mass produced for applications in the telecommunication industry, utilized for signal processing and bandpass filters, and also as touch sensors (12). Its use in biological applications has only been proposed within the last several decades. SAW devices have conventionally been designed to operate in the GHz range but are easily fabricated to produce MHz range resonances (compatible with microfluidic dimensions) with the tradeoff of an increased footprint on the amount of piezoelectric material required. The higher frequencies possible with SAW technology over bulk wave transducers provides finer manipulation capability. SAW transducers consist of a capacitive structure on a piezoelectric substrate (34). When an AC signal is applied, the capacitive structure (the electrode) acts as a current generator and surface waves are generated on the substrate. In order to use the acoustic wave generated by SAW devices, the sample or sample container must be placed on the surface of the piezoelectric substrate. For standing wave configurations, the mounting is a matter of sample cell alignment to the already formed standing wave, as opposed to bulk devices which require precise thicknesses between transducer and channel to form a

standing wave. Due to this, channels can be made of soft materials which have been preferentially used in microfluidics. Spacing between multiple SAW devices can also be made precise and focused, chirped and other designs are relatively simple to create. However, alignment with the channel for standing wave implementations remains a challenge with SAW devices. The implementation of the technology in other industries illustrates potential for commercial translation, although reusable and disposable components are still desirable due to lack of abundance of efficient piezoelectric materials (35, 36). Another benefit of SAW is its power efficiency. As the energy of the SAW is contained within several wavelengths of the substrate surface, there is less energy dispersion than conventional transducers. Based on these advantages, SAW was chosen for this work and as better suited for potential POC applications.

As mentioned previously, acoustic techniques, SAW and BAW, have several disadvantages. Heating in acoustic platforms presents a stability and efficiency issue for the technology but has been controlled previously (28, 37). Another disadvantage of acoustic methods is throughput due to the low flow rates needed to allow acoustic forces to exceed fluid and flow forces. In the past, acoustic methods have been found safe and effective for imaging living tissue and, similarly, have been found to have no damaging effects on function and viability of cells in a controlled system (12). Megahertz frequencies are short enough to significantly limit the potential for cell shearing and lysis. Both acoustic methods (as well as other microfluidic and cell sorting techniques) require equipment to drive flow and amplify signal input from a function generator, and, thus, fall short of the ideal LOC platform. Portability of an acoustic POC platform may be greatly improved from a laboratory setup via building electronics to serve the application and advances in fabrication of miniature electronics, which may allow for a miniature pump and power amplifier. Miniature detection system construction is

well underway with the advent of cell phone microscopy (38). SAW has already been applied to perform an integrated opto-acoustic immunoassay for low-resource environments (39).

Similar to BAW cell separation, SAW has achieved high percent separation in a number of applications, including blood separation, circulating tumor cell separation and bacteria separation (16, 21, 23, 40). Nam et al. explored the use of a conventional SSAW transducer for whole blood separation, achieving 99% separation efficiency of blood cells (16). This experiment is one of a small number of experiments using a SAW transducer in a polymer microchannel for blood separation. The overall design of the experiment, a permanently-bonded trifurcated channel, is similar to that used by Laurell's group, but uses SSAW and specifically studies the recovery of platelets. 74% of platelets were recovered with purity of >98%. This study used relatively low flow rates of 0.25 μL/min and 5 μL/min for sample and sheath fluids, which appears to be much lower than the BAW whole blood separation experiment by Lenshof et al. A design for improving the throughput of whole blood separation with SSAW as well as the theoretical analysis and feasibility is proposed by Wang; however, the concept was not tested with blood (41).

In the area of cell sorting, most other SSAW experiments utilize diluted solutions of cells. Li et al. used tilted SSAW to separate *E. Coli* from red blood cells (23). While the solution was diluted from whole blood concentrations, blood cell concentration was an order of magnitude higher than bacteria content. More than 95% of the bacteria were recovered with greater than 95% blood cell removal, enabling accurate electrochemical analysis. Similar results were obtained by Ai et al. using straight electrodes to separate *E. Coli* from peripheral blood mononuclear cells, although the large cell removal was ~5% lower (42). SSAW has been successfully applied in circulating tumor cell separation as well, using both size-based sorting

and separation by density (21, 40). Apart from blood-based cell solutions, a recent experiment showed the potential of SSAW to process sputum samples, transferring inflammatory cells from liquefied sputum to a buffer solution (43). Upon performing immune-phenotyping on the SSAW-sorted cells, the method was found to enable more accurate results than conventional methods. Cell sorting studies using SSAW typically use frequencies in the range of 7-40 MHz (16, 40, 42, 44).

Both ARF and ASF have been used to manipulate objects below 1 μm in size (18, 45). Collins et al. showed that, from a solution of 100-500 nm nanoparticles, ASF could be used to preferentially concentrate and sort different sizes of nanoparticles (18). While most nano-scale particle manipulations use ASF (46), a paper by Wu et al. explores the limits of ARF for sorting nanoparticles in continuous flow (45). The study finds that size-based sorting is possible for particles down to 500 nm, but the force exerted on 220 nm particles is not significant. An interesting study bonding lithium niobate, where one piece has fabricated nanoslits, was used to create size exclusion based nanoparticle sorting by generating SAW on the opposing piece of lithium niobate (47).

1.3 Microfluidics

In the context of this work, microfluidics refers to the use of micron-scale channels to handle small volumes of liquid. Microfluidics provide precise spatial and temporal control of samples due to their dimensions, made possible by now standard microfabrication techniques. In addition, devices are low cost to manufacture. For these reasons, microfluidics have been proposed as a next generation, portable platform for integrated laboratory analyses in medical applications, as well as others (48, 49).

In microfluidics, fluid behavior becomes highly laminar due to the low Reynolds number generated at this scale (49, 50). It is quite difficult to create chaotic mixing in microfluidic channels without the use of external forces (50). In rectangular microchannels, a parabolic velocity profile exists, called Poiseuille flow, resulting in maximal velocity at the centerline of the channel. Due to the laminar behavior of fluids in microfluidics, transverse mixing only takes place via diffusion (50). With the increased surface area, surface forces (surface tension, van der Waals interactions, etc.) play a large role (49). Two opposing forces also act on particles in the microchannel: shear-gradient-induced lift and wall-effect-induced lift force (51). These forces create lateral forces on particles in the channel based on the channel size and aspect ratio. Since blood and plasma display non-Newtonian and viscoelastic behavior, several additional forces are also present. These forces must be overcome to achieve acoustic sorting.

1.4 Nanoparticle-Based Diagnostics

Diagnostic assays can generally be divided into four steps: sample preparation, recognition, transduction and signal processing (Fig. 2). The research proposed herein constitutes the sample preparation step. The other three steps are based on the assay design. In this work, the assay format of interest accomplishes recognition using metallic nanoparticles functionalized with stabilizing molecules and antibodies or aptamers (the recognition component), which bind to the biomarker of interest. The binding of these nanoparticles to biomarkers is regulated by either competitive binding or requires two nanoparticles to bind to distinct targets on the same biomarker. During the recognition step, an incubation time is observed to allow the binding of the functional groups and biomarkers to reach a steady-state. The transduction step takes advantage of surface-enhanced Raman spectroscopy, a highly specific and sensitive optical method. The Raman signal is directly related to the chemical composition of the sample.

Fluorescence may also be used for the transduction method in this type of assay. The nanoparticles are also functionalized with Raman reporter molecules and/or fluorescent dyes for the transduction element. Depending on the binding state of the nanoparticles with the biomarker, the optical signal is either enhanced or reduced.

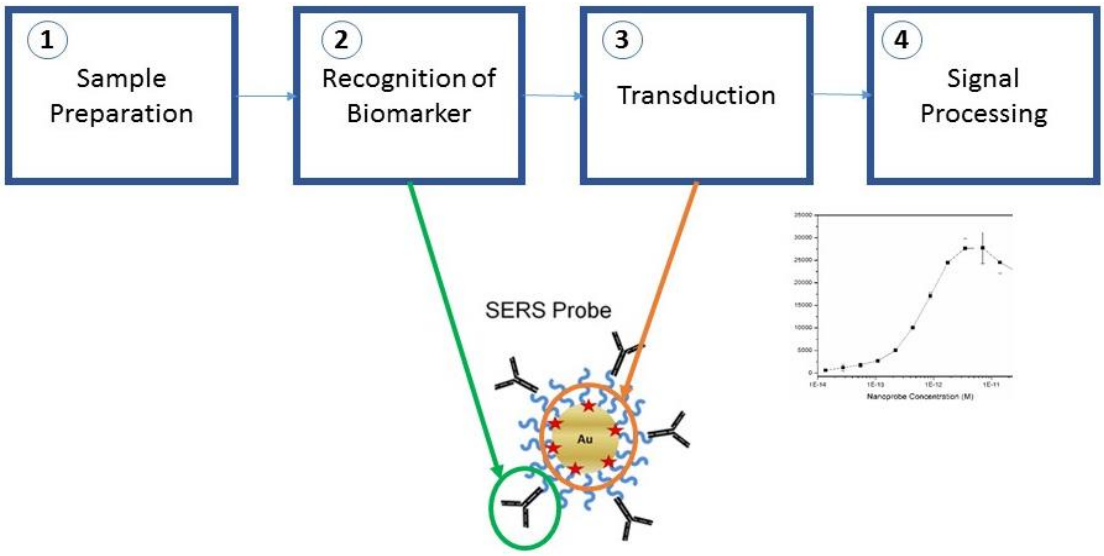

Fig. 2 Diagnostic assays can generally be divided into four steps: sample preparation, recognition, transduction and signal processing. The research herein constitutes the sample preparation step. The purpose of this step is to removing molecules that may interfere with the sensitivity of the measurement. In this work, recognition and transduction are accomplished using functionalized nanoparticles. Binding of the functionalized nanoparticles to the biomarker of interest results in a change in optical signal. The signal change is analyzed through signal processing to determine a diagnosis.

In order to perform blood-based tests in a POC environment, a platform must be used through which to operate on the sample. Microfluidics is one commonly proposed platform. As mentioned in previous sections, additional fluids may be used to dilute the sample or serve as waste streams to enable on-chip microfluidic blood separation. In this work, the use of additional fluid as a waste stream is used to avoid sample dilution and position the sample for efficient acoustic sorting. In microfluidic channels, analyte concentration of adjacent streams is generally diffusion-limited (50). Biomarker concentrations in the plasma may be as low as ng/L (11), making the preservation of concentration a critical parameter for accurate diagnosis. Therefore, when using additional fluids in the system, it is important to measure recovery of the small particles (biomarkers) intended for diagnostic measurement and determination. Since this work tests a single injection assay format, the functionalized nanoparticles used in our application may also be reduced in concentration by similar phenomenon. The particles may interact with other blood components in the channel, resulting in particle loss due to transport in the shadow of larger displaced cells in addition to loss due to diffusion (20, 27). For some assays, nanoparticle concentration is directly related to biomarker measurement via calibration and, as such, recovery of nanoparticles is of interest.

The mechanism of blood separation may also play a role in recovery of small particles and the viability of the platform for the assays mentioned above. Using an acoustic blood separation method, dispersion and further diffusion and particle-particle interaction of plasma, blood cells and assay components (nanoparticles) are possible (50). The nanoparticle size range commonly used (5-60 nm) and biomarker size have not been previously observed to be significantly affected by ARF. However, acoustic streaming may occur in a limited fashion in an ARF experiment and can displace and even sort nanoparticles, as mentioned in the Section 1.2.3

of this chapter. Previous studies have reported significant percentages of biomarker loss (16, 26). Therefore, the selection of experiment parameters, such as flow rate and power, is important. The use of dextrose to increase sheath fluid acoustic impedance has been shown to improve recovery, in addition to other choices of sheath fluid (27, 29). The type of system discussed herein has not been explored in detail for diagnostic use with this nanoparticle-based assay format.

CHAPTER II

MATERIALS AND METHODS

2.1 Surface Acoustic Wave Transducer

2.1.1 Design

In order to design a blood separation platform for eventual POC applications, a SAW transducer was selected as the actuating mechanism. A SAW device provides the advantages of high frequency generation, flexibility and ease of mounting. As the transducer in Nam et al.'s study was effective manipulating whole blood and agrees with the frequency range used in other cell separation experiments (including diluted and whole blood) (10, 16, 23, 26, 42), the frequency of the transducer used in that study (7.54 MHz) was chosen as the design frequency. A standing wave design was chosen due to the additional positional control, repeatability, and increased ARF magnitude provided towards manipulating the sample. A traveling surface acoustic wave (TSAW) transducer, which uses a single electrode, was used for initial tests. In the case of SAW transducers, the resonant frequency of the transducer is directly related to the dimension of the fingers of the inter-digitated structure. SAW-grade, YZ-cut lithium niobate (University Wafers, Inc.), with a speed of sound of (c=3488 m/s), is used as the piezoelectric crystal for its high piezoelectric efficiency. Using the relation $c=f\bullet\lambda$, the necessary design wavelength was found. The aperture of the transducer determines the width of the region where pressure waves are generated. Figure 3 shows the schematic of a simple electrode for an inter-digitated transducer (IDT), which is implemented here to produce a 7.54 MHz pressure wave. Setting λ=115.65 nm yields the electrode design for the SAW and SSAW transducers used in this

work. The aperture of the IDT, the width where directional plane waves are generated, was 10 mm.

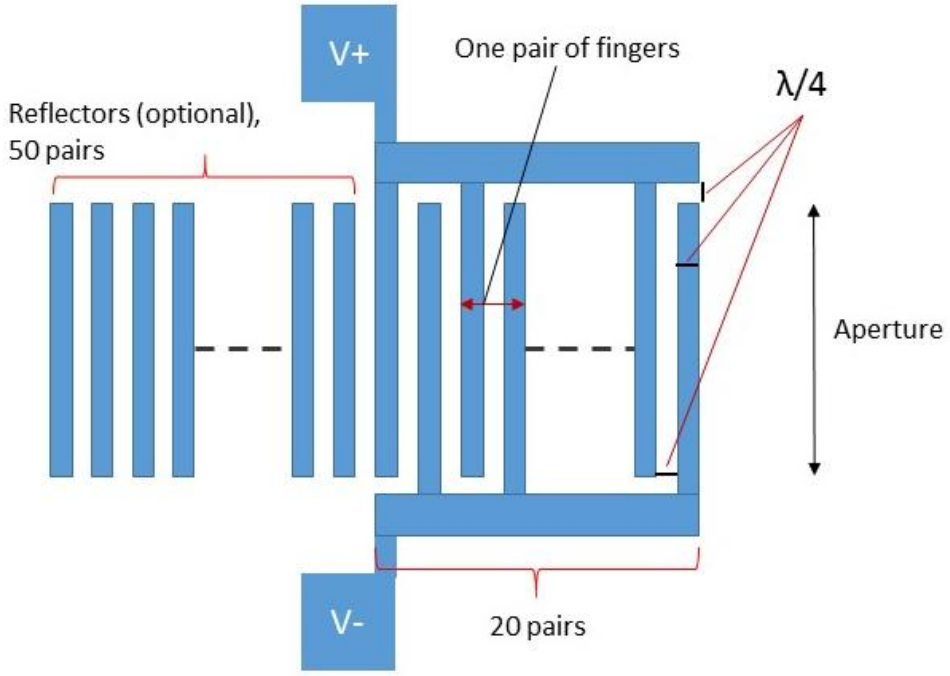

Fig. 3 The dimensions of the electrode of an inter-digitated transducer are a function of the wavelength and related to the desired resonance of the device. The electrode is arranged like two interlocked combs with adjacent fingers called pairs. When voltage is applied, the structure acts as a current generator and surface acoustic waves are produced. The indicated number of pairs is standard to ensure the development of a traveling wave. The dashed lines indicate the repeating finger pattern as well as the transducer axis, along which the pressure wave travels. Adding reflectors is one option to create a unidirectional pressure wave with maximum possible amplitude. Without reflectors, plane pressure waves are launched over the transducer aperture in both directions along the axis.

For a standing wave design, the distance between the electrode pair is a function of the wavelength to ensure the likelihood of interference. Therefore, the distance should be a multiple of $\lambda/2$. While the distance should allow for channel placement on the substrate between electrodes, it should be minimized as possible because, while the wave is traveling along a $LiNbO_3$/air interface and, theoretically, should not attenuate, the SAW amplitude decays slightly over distance. In SSAW transducers used here, the distance was ~18.4 mm.

Photolithography techniques may be used to create the desired pattern. Therefore, a photomask was created using the dimensioning guidelines above. Upon fabrication steps discussed in the next section, the comb (or inter-digitated) structure physically supports frequencies that are multiples of the design frequency when voltage is applied. For each electrode, a traveling surface wave is generated along the surface of the SAW piezoelectric substrate. The photomask designs for 10 mm aperture, 7.54 MHz TSAW and SSAW transducers are shown in Fig. 4.

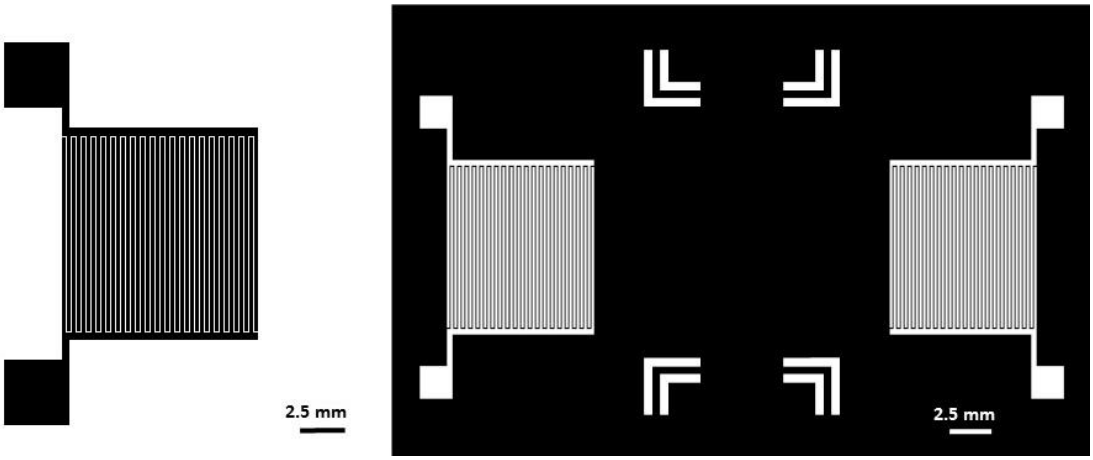

Fig 4. Photolithography masks for a single inter-digitated electrode (left) and a pair of inter-digitated electrodes (right), each with resonance frequency 7.54 MHz. The aperture of the electrodes was 10 mm. Paired electrodes are used for standing wave experiments. Black or clear features are chosen based on the fabrication process used. Alignment markers were included in the standing wave design to guide channel placement.

2.1.2 Fabrication

The SAW transducers were fabricated using a lift-off process (Fig. 5). Etching was also used to fabricate transducers as the protocol was developed but lift-off proved a more reliable process. Transducers were fabricated using 100 mm diameter, 0.5 mm thickness SAW-grade, YZ-cut $LiNbO_3$ wafers. Initially, $LiNbO_3$ was cleaned using piranha solution. However, the thermal stress induced by this process was later found to leave invisible cracks within the material that were discovered in testing. In the lift-off process, photolithography is first carried out. AZ1813 photoresist (Shipley Company) was spin-coated onto the wafer and soft baked for 1 minute at 90°C. The wafer was then UV-exposed using the photomask containing the desired electrode dimensions. The wafer was developed in MF321 developer (Shipley Company). Hard bake was not performed due to difficulty created in later steps. The metallic electrodes were

deposited using an e-beam evaporator. Initial testing used single IDTs, which were fabricated with a variety of metals, discussed below. In the final SSAW devices, chromium was first deposited in a thin layer, followed by a thicker layer of aluminum. Chromium was included to improve adhesion. Finally, the wafer was bathed in acetone to lift off areas of crosslinked photoresist, leaving the two-layer inter-digitated transducer electrodes on the crystal surface. As only part of the wafer was needed to create the transducers, wafers were cut using a dicing saw. Successful single IDTs were mounted on printed circuit boards (PCBs) or on Plexiglas using super glue (Fig. 6A). Successful SSAW transducer fabrications were mounted on 3x6", 1/8" thick glass using an electrically-insulating, thermally-conductive epoxy to serve as a passive heatsink and mechanical stabilization for the fragile crystal wafer, while preventing large shifts in frequency due to coupling (Fig. 6B); for instance, a transducer mounted on aluminum was measured to have a resonance frequency of >9MHz, which is significantly different from the typical structure resonance. Wires for the radio frequency input were attached to the electrode using silver epoxy. The epoxies mentioned above were cured in 70 and 120°C ovens. Occasionally transducers showed signs of cracking after being removed from the 120°C oven; most likely, this indicates small cracks had been induced by previous processes and were propagated by additional thermal stress.

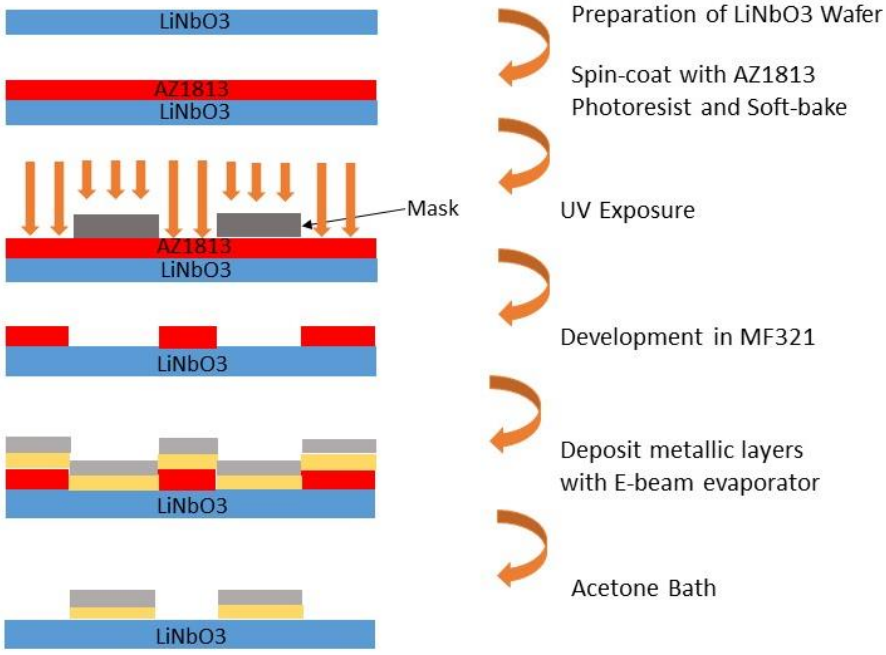

Fig. 5 A lift-off process was used to fabricate the inter-digitated electrodes. Lithium niobate was chosen as the substrate for its high piezoelectric efficiency. First, a photolithography process was used to pattern photoresist with a photomask containing the electrode design. Regions where the electrodes should be deposited are left bare after development. The metallic layers of the electrode were then deposited using an E-beam evaporator. Finally, an acetone bath was used to remove cured photoresist, lifting off the excess metal.

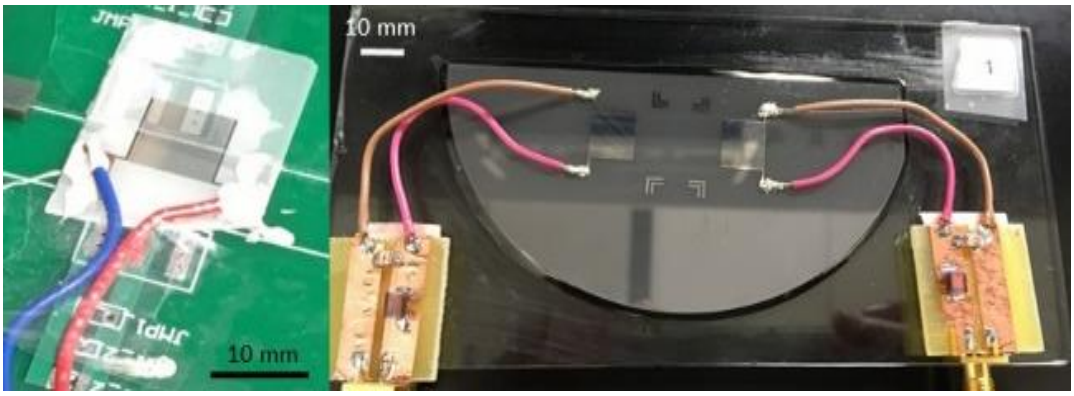

Fig. 6 Fabricated transducers were mounted for stability. TSAW devices were mounted on PCBs (A). The TSAW device is shown with a spacer used for testing of a detachable channel. SSAW devices were mounted on glass to provide a passive heatsink as well as stability (B). The SSAW device is shown with matching circuits added.

Several generations of transducers were constructed prior to the final design. The first generation devices consisted of aluminum-only electrodes, but the design was modified due to adhesion issues. Gold and chromium-gold electrodes were made in an attempt to replicate the composition of transducers used in biomedical experiments in literature (21, 42). The electrode is commonly constructed as a thin layer of chromium, for its strong adhesion, followed by a ten times thicker layer of gold. However, due to increased susceptibility to scratching (and open circuit) and cost, electrode design used chromium-aluminum layers. Aluminum may be made electrically equivalent to gold by changing the deposition thickness of aluminum. Therefore, the resistance of the electrode structure was maintained over fabrications using different metals by assuming a parallel resistor model and using the relation, $R=\rho L/A$, where R is resistance, ρ is the resistivity of the material, L is the length of the structure and A is the cross-sectional area of the structure, to calculate the deposition thickness. However, as noted in other sections, electrode

resistance changes in response to differences in temperature, loading, and changes in other parameters.

2.1.3 Characterization

Individual transducer resonance and loss factor was assessed via S11 measurement with a network analyzer, and used to drive the transducer effectively. S11 is a measure of the power reflected from the load and, therefore, the transmission properties of the load. S11 was collected over a frequency range, including the design resonance, for each electrode. In initial experiments, transducers were not matched. However, in later experiments, simple matching circuits for each electrode were added by using the Smith chart to match the impedance to 50 Ω and tune the resonance frequency such that the two electrodes had similar attenuation values for the chosen resonance frequency. The resonance frequency was chosen as the peak closest to the design frequency which also showed the highest attenuation value and performance experimentally.

TSAW transducers were used to test electrode design, power levels and the effect of frequency. The IDTs were driven by a function generator set to the resonant frequency of a given IDT and a power amplifier (LZY-22+, Mini Circuits). Table 1 below shows the conversion from the power input at the function generator to the power output from the power amplifier. Function generator voltage inputs are used throughout the work to describe the transducer input in experiments.

Table 1. Driving voltage and power through the power amplifier. Voltage inputs at the function generator are used to describe transducer voltage in experiments. Theoretical values of voltage and power at the power amplifier output are given in this table.

Voltage In (mVpp)	Power In (W)	Voltage Out (Vpp)	Power Out (W)
100	0.000025	14.125	0.499
200	0.0001	28.251	1.995
300	0.000225	42.376	4.489
400	0.0004	56.502	7.981
500	0.000625	70.627	12.47

Plastic beads (5-10um) were suspended in water and droplets were placed on a cover glass and coupled via ultrasound gel to the surface of TSAW transducers in front of the electrode. The cover glass was pressed as close to the transducer surface as possible and excess ultrasound gel was removed to prevent additional loading and attenuation. In this case and that of the channels designed in the next section, distance from transducer surface to the channel material should ideally be 1-2λ and less than 10λ in order to couple most of the SAW since amplitude decreases with distance from the surface. The voltage was varied between 0-550 mV_{pp} to observe generated ASF and the resulting speed of particle mixing and centrifugation.

Piezoelectric transducers have transmission properties sensitive to changes in temperature and loading. Heating of the transducer substrate and, subsequently, the sample may cause changes in the sample speed of sound and electrode resistance, resulting in changes in resonance. The heating of SSAW transducers was measured using an IR camera. The temperature increase

from ambient (~22-23°C) was measured after 60 seconds of applied voltage, ranging from 100-500 mV_{pp}.

2.2 Microfluidic Channel

2.2.1 Design

Several microfluidic channel designs were used throughout this work. A straight, single inlet, single outlet channel (250x86 um) was used for some initial experiments including comparison of channel designs using TSAW (Fig. 7A). For other TSAW experiments, a two inlet, two outlet channel (150x50 um) was used (Fig. 7B). In this case, cell displacement experiments were performed to evaluate which design had higher power transmission. Finally, two trifurcated channel designs were used for SSAW testing. The first of which had 150 μm wide branched channels (Fig. 7C) while the second had 50 μm wide branched channels (Fig. 7D). Branched channel were at 30 degrees to the central channel. The width of the main channel was 150 μm and the height 50 um, with channel lengths of 15 to 25 mm. The entrance length for laminar behavior was found to be <<1mm, and was not a concern at the channel lengths used for acoustic manipulation.

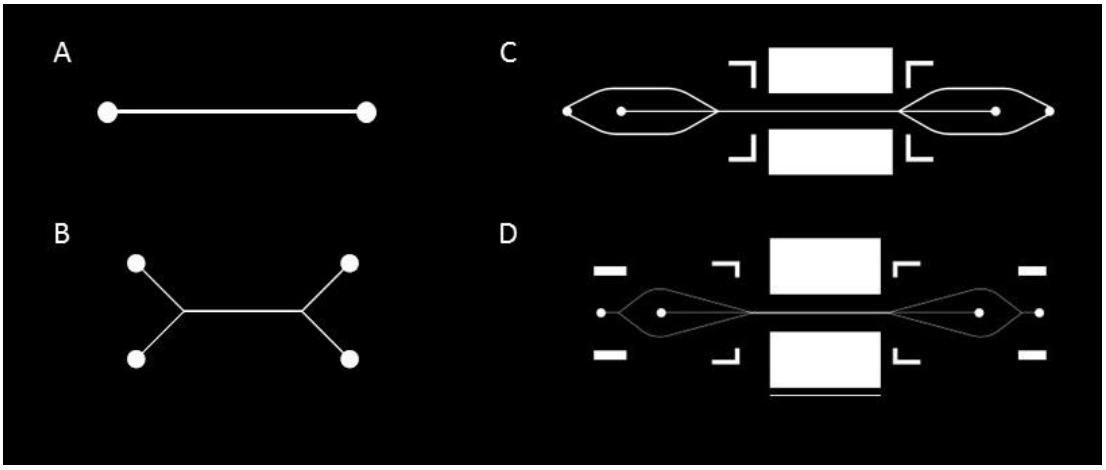

Fig. 7 Multiple microfluidic channel designs were used throughout this work for preliminary experiments (A,B) and SSAW blood separation experiments (C,D). Single inlet, single outlet channels were used for comparison of detachable channel designs (A). Two inlet, two outlet channels were used for testing TSAW for blood separation (B). Trifurcated channels were used for final blood separation experiments (C,D). The primary difference between the designs is the branch channel width which was 150 μm for design C and 50 μm for design D. Alignment markers align to markers on either or both of the PDMS pillar design, discussed below, or the SSAW transducers. Several main channel lengths were tested as well.

A TSAW transducer was used with design A and B in Fig. 7 as a potential blood separation platform and to test detachable channel designs. Using TSAW would limit the amount of SAW substrate necessary to fabricate a transducer. In addition, the total translation of particles would not be limited by the nodal positions (35).

The SSAW microfluidic channel was designed to support cell sorting via standing wave and also to support sheath flow configuration as these designs have performed well in previous experiments (10, 16, 23). By injecting the sample (whole blood) in the middle inlet and the sheath fluid (PBS) in the outer two inlets, the blood sample is hydro-dynamically focused and located in the streamline with velocity greater than zero, limiting the shear seen by the cells and

forces at the channel wall that may dominate over the ARF. The low flow environment required for acoustophoresis must be separated as possible from the other forces at the channel wall to enable efficient and predictable sorting. Along the length of the main channel, where all fluids converge, blood cells are moved to the nodal positions in the sheath fluid streams and discarded out of the outer two outlets when the transducer is actuated. The blood plasma is meant to continue in its central streamline through the central outlet for collection. PBS is selected as the sheath fluid because compatible with physiological conditions. Some common challenges in blood experiments in microfluidics include pulsation and clots which disturb the laminar flow environment. For this reason, anti-coagulated blood for all experiments will be used within three days of being drawn.

To make use of the standing wave, the microfluidic channel should have a width close to or greater than $\lambda/2$, so that the nodes locate particles in the PBS streams. The main channel width for the cell sorting experiment was selected to be 150 um, while the height was 50 um. The height was chosen such that, in combination with the coupling layer, the propagation distance of the acoustic wave into the sample container was less than several wavelengths, because the wave is known to attenuate after several wavelengths (35, 36). Fig. 8 shows the flow scenario.

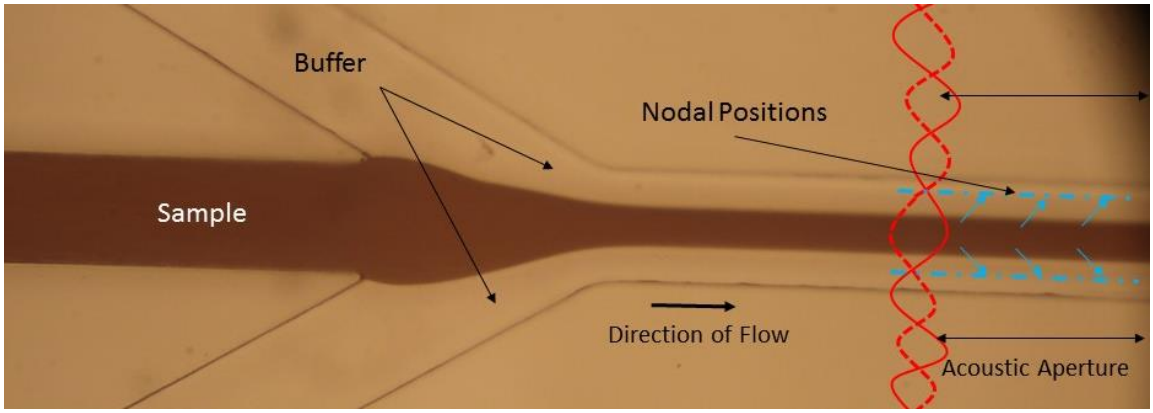

Fig. 8 Flow scenario for standing wave blood separation experiment. The blood sample is located in the middle stream, while PBS serves as the sheath fluid. When the SSAW transducer is actuated, nodes, areas of low pressure, are formed, generating ARF that effects blood components in a size-dependent fashion. Nodes are formed along the length of the channel which is positioned such that the flow direction is perpendicular to the propagating waves from the apertures of the SAW electrodes. The channel width was selected such that half the wavelength of the SAW would locate nodes in the buffer fluid streams.

Unlike bulk wave transducers, SAW transducers can form SSAW independent of the sample placed between electrodes, assuming it supports acoustic propagation. Due to this property, a softer material such as a polymer may be used to construct the microfluidic channel, as it is not needed to aid in standing wave formation. This allows rapid prototyping, avoids time-consuming processes such as glass etching, and provides high accuracy in channel dimension. In this work, polydimethylsiloxane (PDMS), an optically-clear silicone-based polymer, is used as the channel material.

The design discussed above describes the design of the channel lumen. To complete the channel, it must be bonded to something. Many acousto-fluidic experiments bond the channel directly and permanently to the SAW substrate. However, this does not allow use of the

transducer for multiple experiments, especially for biological experiments. Since, for testing, transducer reuse is desirable and as the yield of our fabrication protocol was low, channel designs making use of a temporary bond were chosen. Transducer reuse would also be desirable for a POC application to keep cost down. In this format, the channel, containing the blood sample, is disposable.

For a SAW microfluidic experiment, there must be propagation of the wave from the substrate surface into the channel material and sample. The first of the temporary bond channel designs was taken from O'Rorke et al. (36) The design bonds the PDMS channel to a glass coverslip, and the structure is coupled to the transducer by ultrasound gel. The pressure wave at the channel is a Lamb wave, which is similar to a bulk wave in its behavior. The second temporary bond channel design was taken from Ma et al. (35) The design uses a pillar structure to guide the acoustic wave into the channel by bonding the PDMS channel to a thin PDMS pillar-patterned layer which seals the channel. The pillar is aligned to the channel and then to the aperture of the transducer. Pillar widths tested were 0.6 and 1.5 mm with lengths of ~12 mm, which is greater than the acoustic aperture to take into account misalignment and refraction of the waves. Height of the pillar was 25 um, with an overall layer thickness of ~50 um. This design uses conformal coupling of the PDMS channel to the transducer surface. Another interesting design by Witte et al. uses glass slides patterned with photoresist to create a detachable channel and is coupled by fluid (52). This design was not explored here because biocompatibility, fabrication and performance were in question. There may be acoustic benefits to using a resonant cavity; however, the fluid coupling aspect is tested in O'Rorke's design which addresses attenuation of the wave in such a layer. Fig. 9 shows the separable channel concepts tested here.

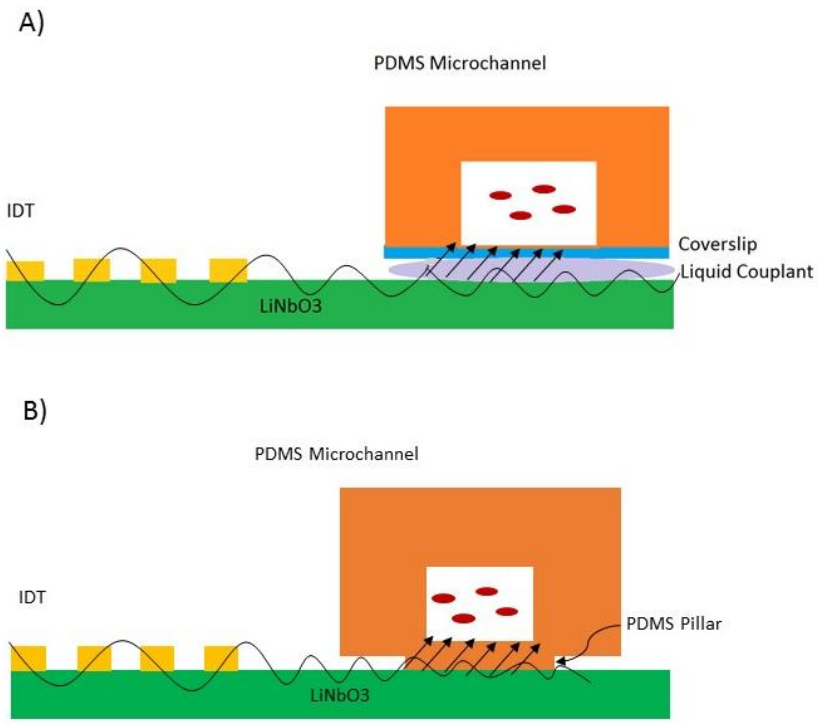

Fig. 9 Transducer-separable channel designs for SAW experiments. The first design used a PDMS channel bonded to a glass cover slip (A). The channel was coupled to the transducer via ultrasound gel. The second design used a PDMS channel bonded to a thin pillar structure made of PDMS. The channel was coupled to the transducer by conformal bonding.

2.2.2 Fabrication

To create PDMS channels, master molds are first created using photolithography. The process is described in Fig. 10. Three inch silicon wafers are cleaned using acetone and IPA, and are then dehydrated in a 120°C oven for a few minutes. Wafers are allowed to cool before pouring a small amount of SU8 photoresist (Microchem) onto the center of the wafer. For the channel mold, SU8 2050 is used to achieve the 50 μm height. For the pillar mold, SU8 2025 is

used. These photoresists are very viscous; to avoid introducing air bubbles and wasting photoresist, SU8 should be poured very slowly without moving the bottle. The resist was spread over the wafer to wet most of the surface by tilting the wafer. For the channel mold, the following protocol was used. The wafer was loaded into a spin coater, centered on the chuck and spun using the following spin sequence: ramp to 500 RPM at a rate of 100 RPM/sec, spin at 500 RPM for 10 seconds, ramp to final spin speed of 4000 RPM at a rate of 300 RPM/sec, spin at 4000 RPM for 30 seconds. The wafer was then soft-baked on a hot plate at 65°C for 5 minutes and 95°C for 9 minutes. Wafers were allowed to cool. Using the photomask in Fig. 8, the wafer was brought into contact with the mask and UV exposed for 66 seconds. Post exposure bake was performed at 65°C for 5 minutes and 95°C for 6 minutes. Wafers were allowed to cool. Wafers were developed using SU8 developer for ~90 seconds, rinsed in fresh developer, washed with IPA and dried with nitrogen. Structure height was measured as 50+/-5 μm using a Dektak profilometer. The 25 μm height pillar mold was fabricated similarly using SU8 2025. For the pillar mold, the final spin speed was 3700 RPM. Soft bake times were 3 minutes at 65°C and 6 minutes at 95°C. The wafers were UV exposed for 60 seconds. Post exposure bake times were 1 minutes at 65°C and 6 minutes at 95°C. Structure height was measured as 25+/-5 um. Molds that fell within the desired height range were accepted and used for fabrication of channels. These molds were coated with methyltrichlorosilane using a dessicator before use. This coating allows for the spin-coated PDMS layer to be removed from the mold.

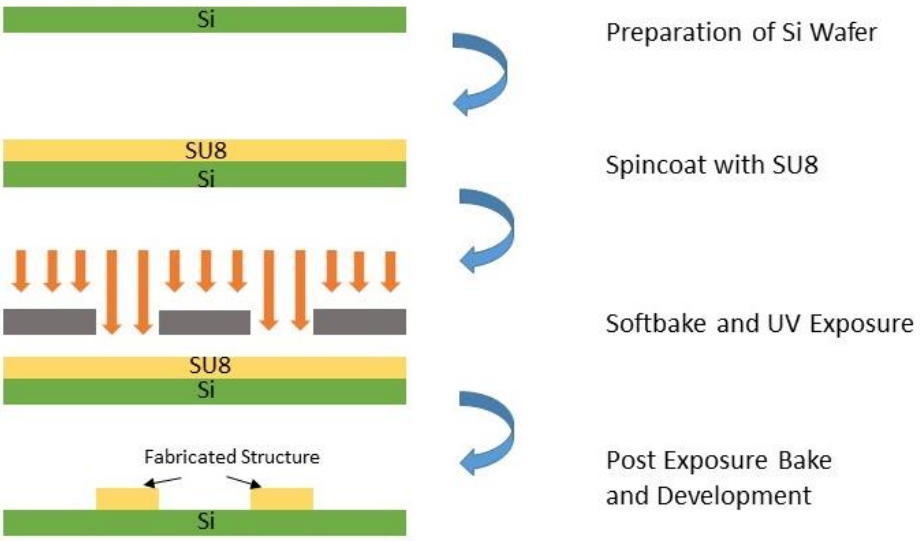

Fig. 10 Molds for the microfluidic channels were fabricated using a photolithography process. Photoresist was spun on silicon wafers to create the desired channel height. Soft-bake was performed. Photomasks of channel designs shown in Fig. 7 were used during UV exposure to cure the photoresist at the location of the channel design. The wafers were baked again and developed to leave the negative of the channel.

To create PDMS channels, channel molds were taped to the bottom of glass petri dish. PDMS was prepared using the Sylgard 184 Elastomer kit, mixing PDMS base with curing agent in a 10:1 ratio. The solution was mixed well, poured into the glass petri dish on top of the channel mold, and dessicated for 30 minutes. Upon removal, remaining bubbles were removed with a pipette. The PDMS was baked at 90°C for 20 minutes to cure. Using 25-30 g of PDMS generally resulted in 3-4 mm height channel, which was useful for later tubing installation. For the PDMS pillar molds, 5 g of PDMS was prepared and spin-coated at 1500 RPM for 30s to produce a ~50 μm layer and baked on a hot plate for 20 minutes. PDMS channels were prepared

by carefully cutting around the silicon mold and removing the patterned PDMS. This was cut into separate devices by cutting along the rectangular features of the pattern. Inlets and outlets were made using a 1 mm punch and the cores removed. The channels and spin-coated pillar molds were cleaned with IPA and plasma-treated. The plasma-treated surfaces were aligned by eye and, using the alignment markers, brought together to bond and baked at 90°C to enhance the bonding. Methanol diluted with water 1:1 may also be used to extend the plasma and allow easier alignment but sometimes resulted in pockets between the bonded surfaces. Finally, the channels were cut from the mold. To make the glass-PDMS channels, cleaned PDMS channels and cover glass were plasma-treated, surfaces brought together to bond, and baked at 90°C for 20 minutes. The glass-PDMS bonding was able to use an unregulated plasma cleaner, but the PDMS-PDMS bonding process required careful control of pressure and oxygen (and a plasma cleaner with regulation capability). Stiff PTFE tubing (SWTT-28-C, Component Supply Co.) was installed in all inlets and outlets. The tubing was selected based on its small dimension that fit into the 1 mm punch. Fig. 11A-C shows the channel master mold, the pillar master mold spin-coated with PDMS, and the PDMS channels bonded onto the pillar mold. Fig. 11D shows the error in manually aligning the channel to 0.6 μm pillar. To improve alignment here and when aligning with the transducer, an advanced alignment system is required.

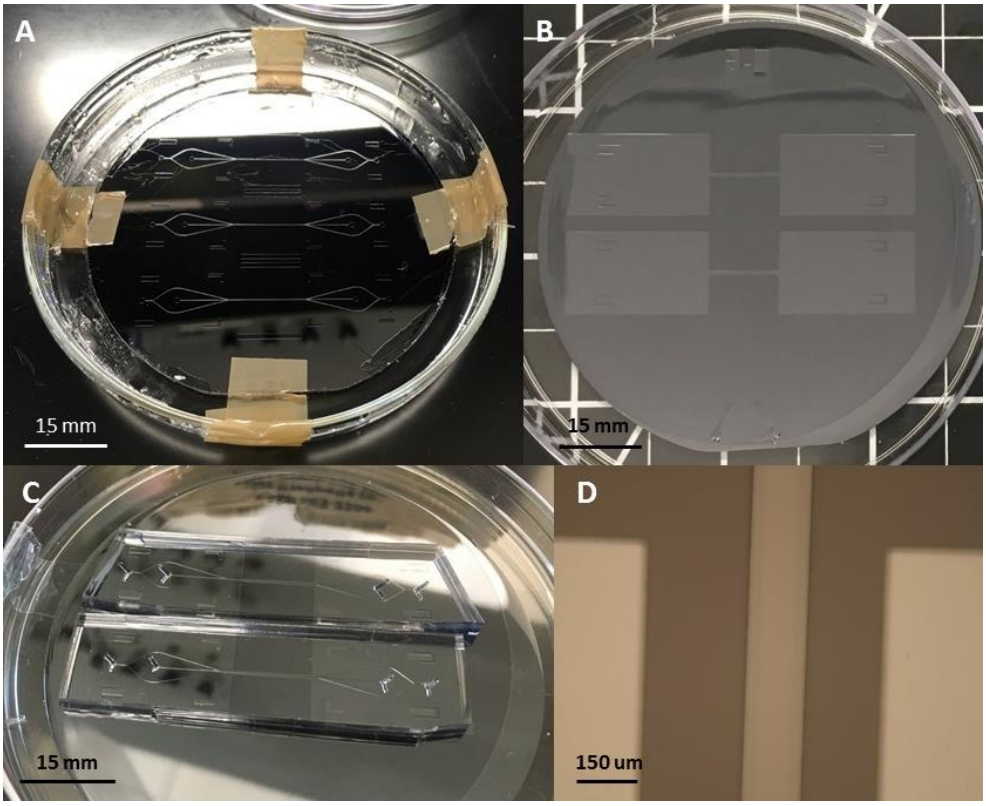

Fig. 11 Fabrication of channel devices. PDMS was poured over master molds (A) to create the top of the channel. Individual channels were cut from the molds and plasma bonded to either glass or spin-coated PDMS on PDMS pillar mold (B). Bonded PDMS pillar devices are shown in (C). PDMS channels were manually aligned to the pillar structure, resulting in alignment error as shown in (D).

2.2.3 Characterization

Flow will be driven by syringe pumps (11Plus, Harvard Apparatus) capable of pumping in the range of 0.2 μL/min – 1 ml/min to provide a range similar to SAW experiments in literature (26, 29, 42). The ratio and value of pump flow rates of the sample and sheath fluid were iterated to create three laminar streams that allowed for effective acoustic sorting (where most cells are significantly displaced). Several channel lengths were also tested with different

flow rates to look at the presence of diffusion. To initiate laminar streams, the pumps were manually pushed to clear any initial clogging or bubbles. Having a burst function on the pump would solve the non-uniformity in this process. Components and settings for the flow system were evaluated by calculating the local flow rate throughout the system using the simple relation $A_1v_1=A_2v_2$. Table 2 below shows the examples of how the flow rates through the system change when channel dimensions and components are changed. The reduction in flow rate at the trifurcation for the 150 μm branch width design initiated the design change to 50 μm branch width since a reduction at the outlets could allow for mixing or diffusion to occur after sorting. Changing the syringe size and diameter setting in the pump was also found to reduce flow rates. Using a 3 mL syringe and its diameter in the pump and similarly when using a 1 mL syringe, the flow rate appeared too fast and resulted in inconsistent acoustic sorting results. By using a 1 mL syringe and setting the pump diameter to that of the 3 mL syringe, the flow rate in the channel was reduced by a factor of approximately three and pulsing from the pump mechanics was limited. This use of the pump allowed for more consistent separation results and less pulsation.

Table 2. Flow rate throughout the microfluidic device when parameters of the flow system, including tubing size and branch channel width, are altered.

Components	Fluid	Pump Flow Rate Setting (ul/min)	Tubing In Flow Rate (mm/min)	Inlet Flow Rate (mm/min)	Main Channel Flow Rate (mm/min)	Outlet Flow Rate (mm/min)	Tubing Out Flow Rate (mm/min)
Small Tubing, 50 um branch width	Sample	3	8.02	365.76	365.76	365.76	8.02
	PBS	10	26.735	609.6	609.6	609.6	26.735
Small Tubing, 150 um inlet width, 75 um outlet width	Sample	3	8.02	121.92	365.76	243.84	8.02
	PBS	10	26.735	203.2	609.6	406.4	26.735
Larger Tubing, 50 um branch width	Sample	3	1.847	365.76	365.76	365.76	1.847
	PBS	10	6.156	609.6	609.6	609.6	6.156

The glass-PDMS and PDMS-PDMS channels were compared using the channel design from Fig.7A and a TSAW transducer. A single inlet, single outlet channel was used to prevent displacement from being confused with flow alterations in the comparison of detachable designs. A TSAW transducer was used because its effect, a unidirectional force on particles, was expected to be more obvious than ARF exerted by standing waves. Blood was used as the sample due to sedimentation of polystyrene beads in experiments lasting longer than several minutes. Diluted blood was used to more readily observe displacement and distribution of particles. 10X blood was injected as the sample and power requirement for sample displacement was observed under a microscope. The voltage was varied in 50 mV_{pp} intervals from 100-550 mV_{pp}. Successful displacement was defined as clear deflection away from the TSAW transducer, where greater displacement occurs as the sample moves a greater distance through the acoustic aperture. The flow rate was 2 μL/min.

2.3 Integrated System

The work herein develops a sample preparation platform for implementation of a single injection assay format, where the blood sample is combined with assay components before sample preparation. Fig. 12 shows the general concept of the integrated platform. A detachable microfluidic device is mounted between two SAW electrodes on the SAW substrate. Laminar streams of a whole blood sample combined with functionalized nanoparticles and PBS are formed in the channel. Upon actuation of the transducer, blood cells are removed and plasma containing functionalized nanoparticles is collected from the center outlet. Optical measurement of the nanoparticle assay is then performed to yield a diagnosis. A single injection assay format is advantageous for two reasons. The first is that by reacting the sample prior to sample preparation, the signal readout is more likely to be proportional to the original biomarker content, since when sample preparation is performed first, any biomarkers lost in the process cannot be taken into account. The second reason is that bioactivity of biomarkers and their binding to assay probes will be greater when the sample is fresher.

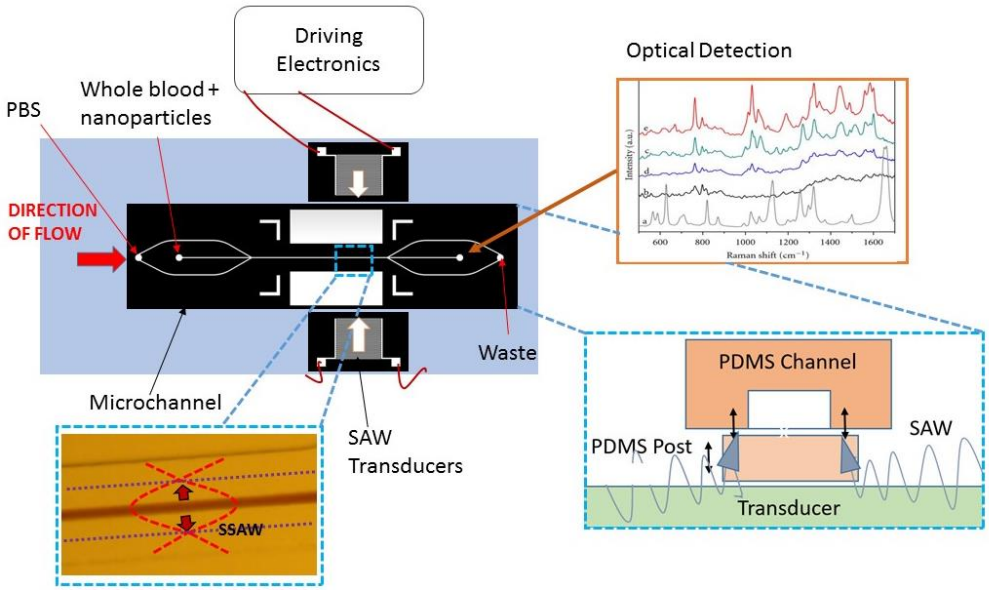

Fig. 12 General concept of the integrated platform. A detachable microfluidic device is mounted between electrodes on the SSAW substrate. Laminar streams of a whole blood sample combined with functionalized nanoparticles and PBS are formed in the channel. Upon actuation of the transducer, blood cells are removed via the standing wave and plasma containing functionalized nanoparticles is collected from the center outlet. Optical measurement of the remaining sample is then performed to yield a diagnosis.

In order to design a blood separation platform for eventual POC applications, a SAW transducer was selected as the actuating mechanism. Transducers were driven by a function generator and power amplifier (LZY-22+, Mini Circuits). During experiments, the highest driving input voltage to the power amplifier corresponded to the 1 dB compression point of the amplifier (~563 mV_{pp}). A laptop power supply was used for the amplifier. The transducer was mounted on a reflectance bright-field microscope with camera-capture. Syringe pumps were located to one side of the microscope. A 10X Leica objective was used to visualize the experiment. Fig 13 shows the setup for the initial SSAW blood separation acoustic experiments.

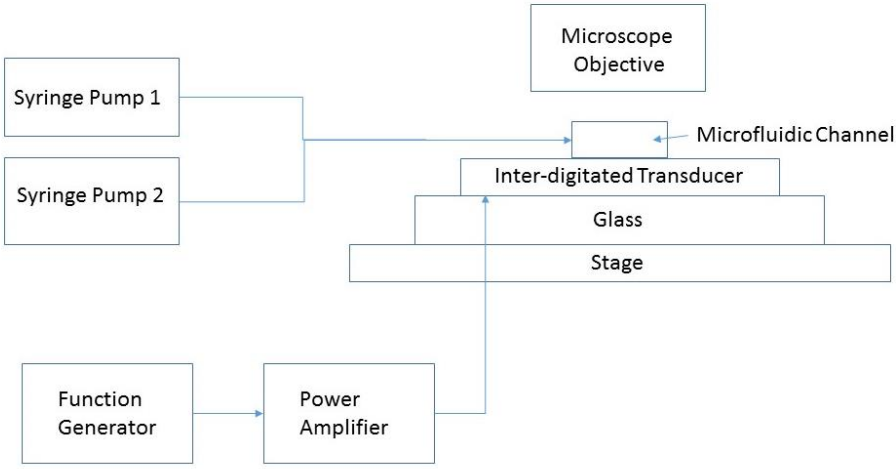

Fig. 13 Equipment used in initial blood separation experiments. Pumps were used to drive fluids at different flow rates. A function generator and power amplifier were used to drive the transducers. Experiments were performed under to microscope to visualize the effect of the transducer on the sample.

Since the acoustic separation experiment is frequency-dependent, the spectrum of the power amplifier output was measured, using a network analyzer and power attenuator, in order to check the magnitude of harmonics introduced to the output by the power amplifier, in- and outside of the amplifier's linear range. Fig. 14 shows that the amplitude of harmonics is at least an order of magnitude less than the fundamental frequency. Amplitude of harmonics increased near and beyond the linear range of the amplifier (with input voltage exceeding 563 mV_{pp}). Based on this measurement, harmonics interfering with the primary ARF frequency was not a concern.

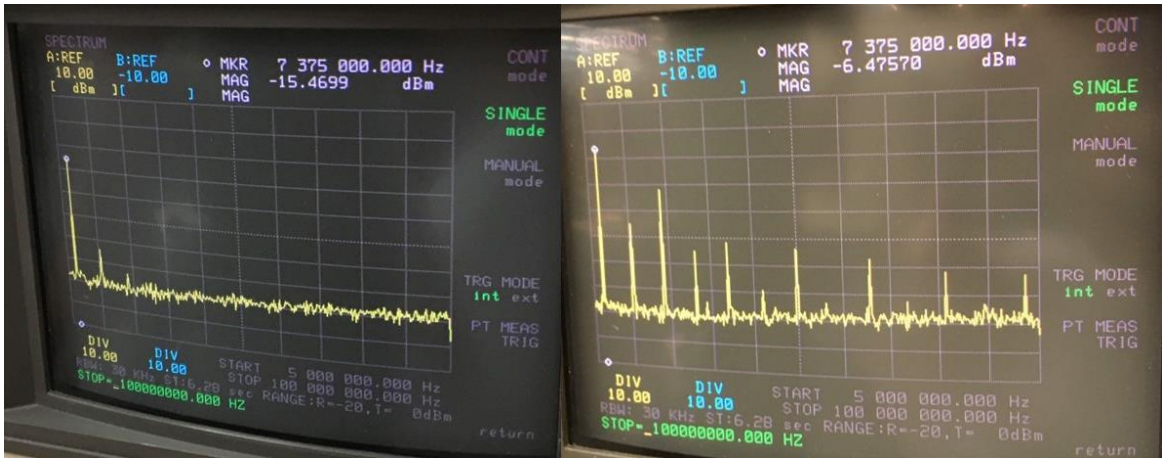

Fig. 14 The output S11 spectrum of the LZY-22+ power amplifier was measured using an attenuator for an input sine wave at 7.375 MHz at 50 mV_{pp} (left) and 800 mV_{pp} (right). Within and outside the linear range of the amplifier, the contribution of harmonics was seen to be at least an order of magnitude below the fundamental.

For the SSAW experiment, the microfluidic channel containing the sample was placed on top of the transducer between the electrodes and approximately aligned with the alignment markers on the transducer (Fig 15). Syringe pumps were placed as close to the microscope stage as possible to limit the tubing length and distance for the sample to travel at low flow rates. Centrifuge tubes were taped to short outlet tubes for collecting the fluids. The setup of the channel for the TSAW experiment is shown in Fig. 16.

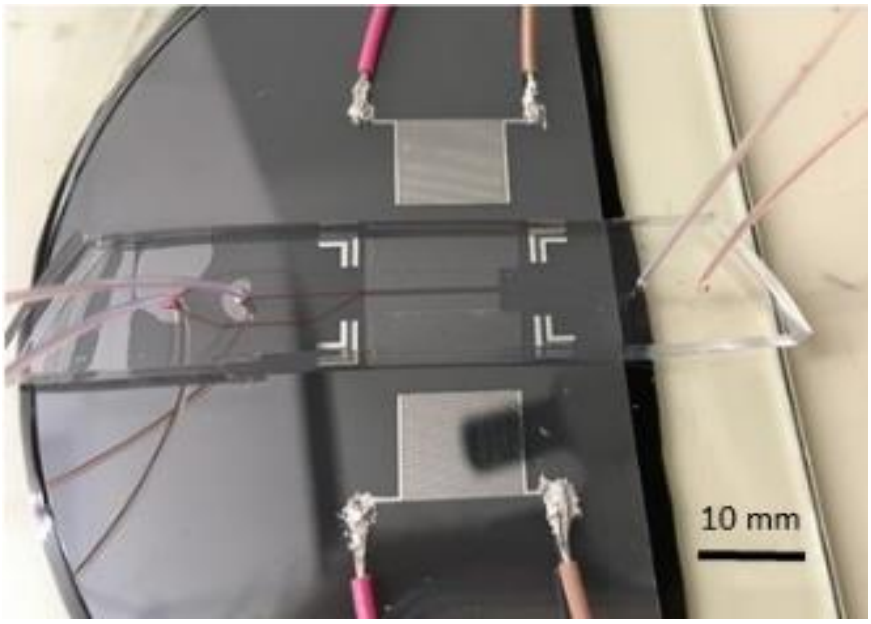

Fig. 15 PDMS-PDMS microfluidic channels were coupled to the SSAW transducer via conformal bonding.

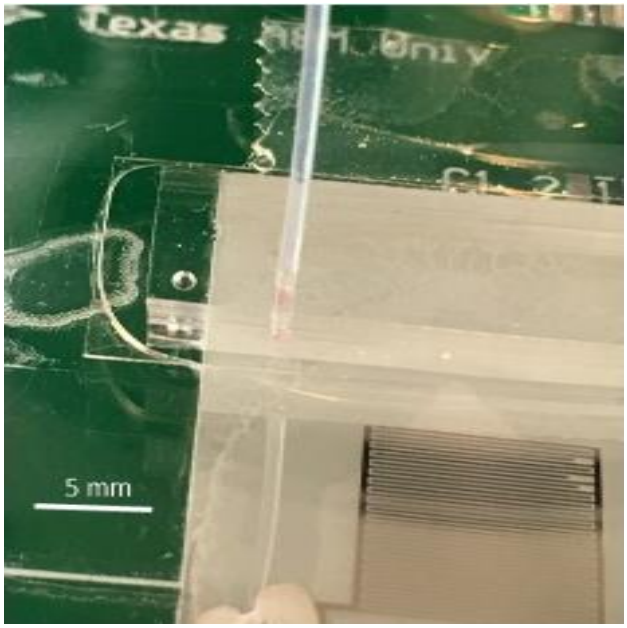

Fig. 16 Glass-PDMS microfluidic channels were coupled to a TSAW transducer via ultrasound gel.

After initial acoustic experiments, it was concluded that long-term cell sorting experiments would require temperature stabilization of the transducer. A temperature regulation system was constructed, consisting of a Peltier element (71012-506, Laird Technologies), heat sink, fan, thermo-conductive pads, and LabVIEW–controlled feedback system. The design was based on systems used by Augustsson et al. and Shilton et al. (28, 53) The Peltier element creates a temperature gradient that allows heat to be drawn away from the component on the cold side of the element. The Peltier element used here was selected to have an area (30x60 mm) corresponding to an area slightly larger than the area of the SSAW that heats during the acoustic experiment as visualized by an infrared camera. The optimal power for the Peltier element was determined by experimentation. The Peltier element was coupled to the transducer using thermo-conductive pads. A heat sink was positioned on the hot side of the Peltier element to drain the heat from the element. A 64 CFM fan was positioned to funnel air through the heatsink to remove the heat from the system. Power supplies were added for the fan and Peltier element. The temperature regulation components had to fit under the microscope objective and, therefore, were selected to have limited height. A larger heat sink should be custom made for this application. Fig. 17 shows the components that were added to the transducer setup.

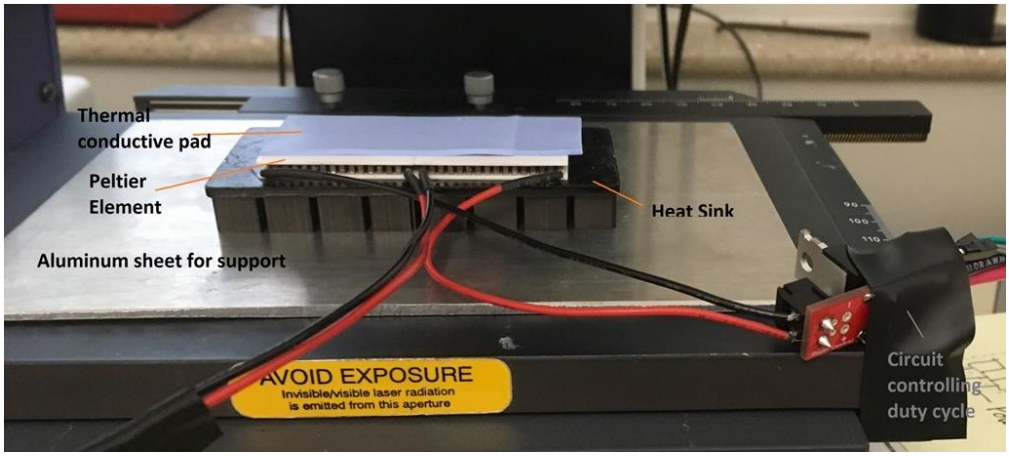

Fig. 17 A Peltier element and heat sink were placed underneath the transducer and microscope for regulation of the transducer temperature. Thermally conducting pads were used to transfer heat between the transducer and Peltier element. Power to the Peltier element was regulated using a switch controlled by custom PID software.

The LabVIEW software implemented a PID loop feedback system, controlling the duty cycle of the Peltier element and using a thermocouple to measure the transducer temperature to form a closed loop control system. PID stands for proportional integral derivative, which describe the different responses used by the system to reach the set point and determining how a parameter, such as the duty cycle, needs to correct to get to the set point. In this system, the temperature of the transducer is the process variable and the duty cycle is the actuator output. Three coefficients K_p, K_i, and K_d are associated with the proportional, integral and derivative responses which together determine the actuator response using the error between the process variable and the set point at a given time. The proportional component, K_p, defines the ratio of the output response to the error signal. The integral component sums the error over time providing a term which slowly brings the system to steady-state, near the set point. The

derivative component, K_d, uses the rate of change of the process variable to decrease the actuator output. Manual tuning of these coefficients for this system was used. Since the transducer heated at a high rate, usually K_p was set to 75, while K_i and K_d were set to 0. While use of K_i and K_d produced a stable temperature, with little oscillation, these coefficients were not efficient when the transducer was actuated. Using only K_p produced oscillation in the duty cycle of the Peltier element as well as the temperature but the response time was sufficient. The variation ranged depending on the experiment from 0.2 to several degrees. The Peltier element was only turned on when the temperature was above the set point. For a slower-changing temperature, which applied to a few experiments that were able to use power levels slightly lower than that used the majority of the time, coefficients of $K_p=8$, $K_i=1$ and $K_d=0.005$ sufficed. Fig. 18 shows the LabVIEW interface for the temperature regulation system. The temperature of two thermocouple probes is displayed and the input to the PID loop can be switched between probes. The second probe was usually used to show ambient temperature or as a time marker. The probes were powered and read using a NI DAQmx. The DAQmx also controlled a MOSFET switch for duty cycle control.

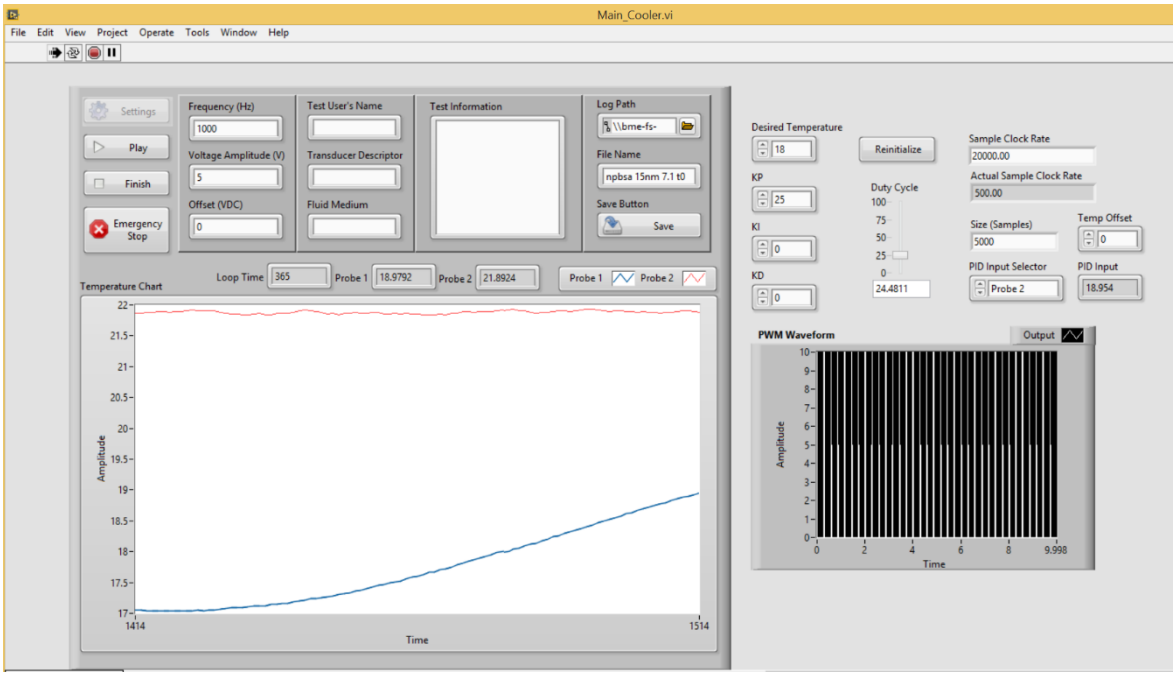

Fig. 18 LabVIEW user interface for temperature regulation system. Thermocouples were used to measure transducer temperature and as input to a PID loop which resulted in an output duty cycle. The set point and PID coefficients were set in the software.

The LabVIEW software implemented a PID loop feedback system, controlling the duty cycle of the Peltier element and using a thermocouple to measure the transducer temperature to form a closed loop control system. Figs. 19 and 20 show the transducer setup on the microscope stage with the cooling system components added. Since the electrode design used here generates acoustic waves and heat both in front and behind the electrode, the thermocouple probe is placed behind one of the electrodes and held in position with a thermally conductive pad. The probe is placed close to the location of the hot spot formation when the transducer heats but not in contact with the electrode or neighboring wires. Fig. 21 shows all of the equipment used and the setup for the temperature-regulated blood separation experiment. The temperature regulation system

was used in blood separation experiments to evaluate the ability of the system to cool the transducer and maintain the transducer temperature for longer experiments.

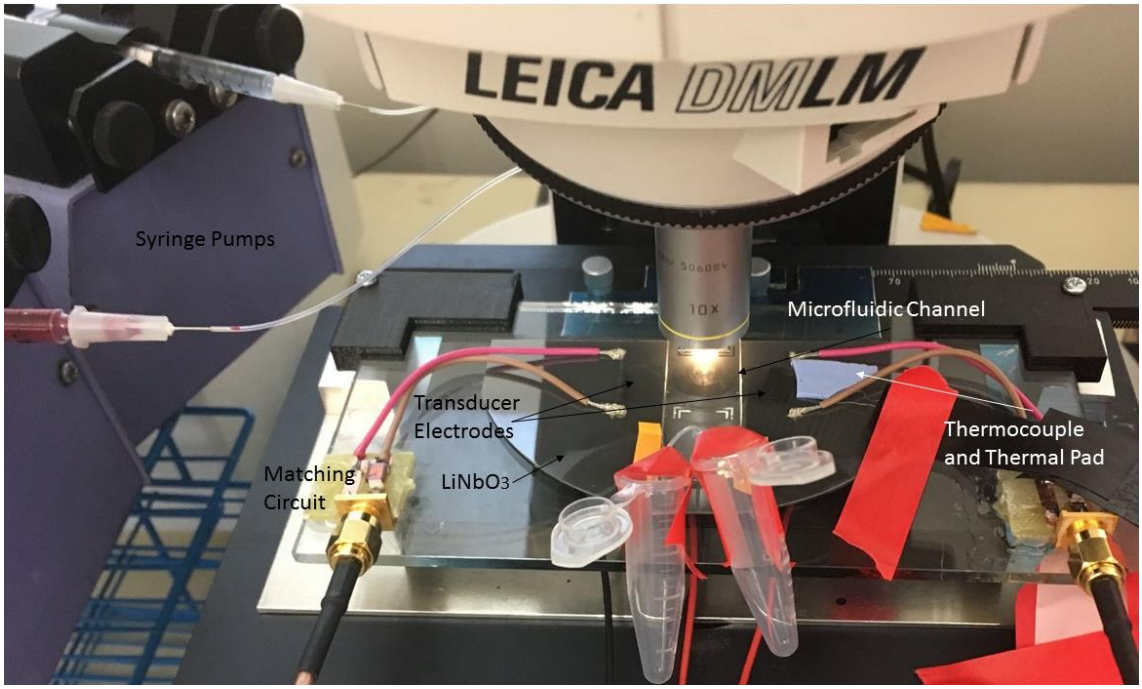

Fig. 19 Top view of the transducer setup under the microscope with temperature regulation components.

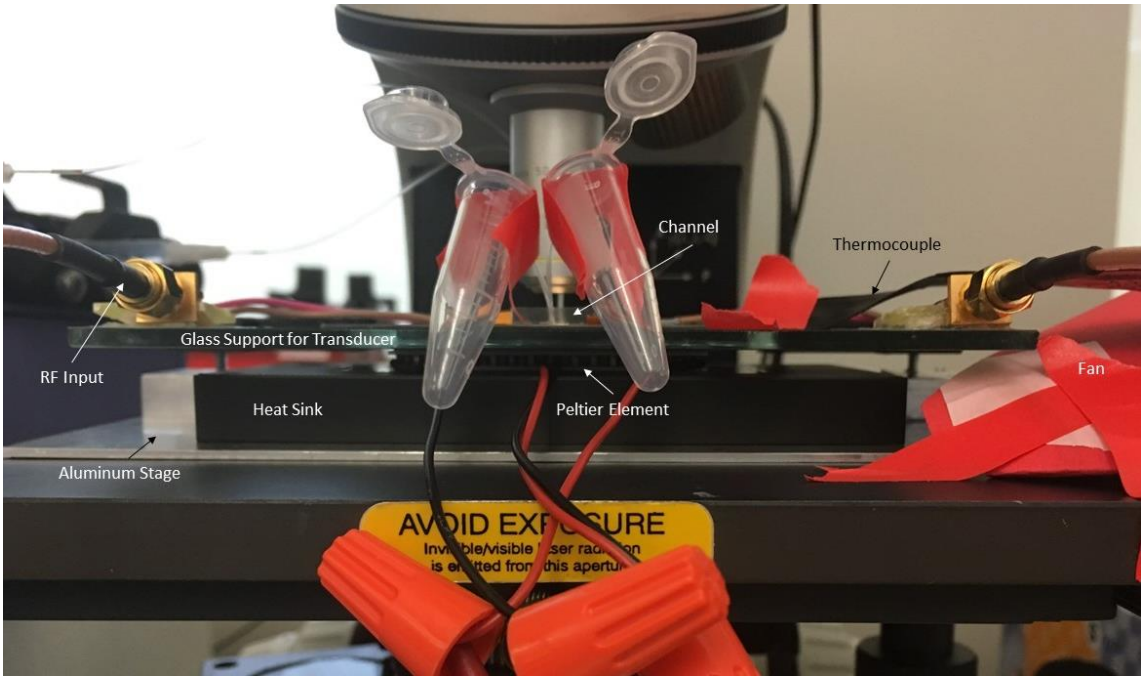

Fig. 20 Side view of the transducer setup under the microscope with temperature regulation components.

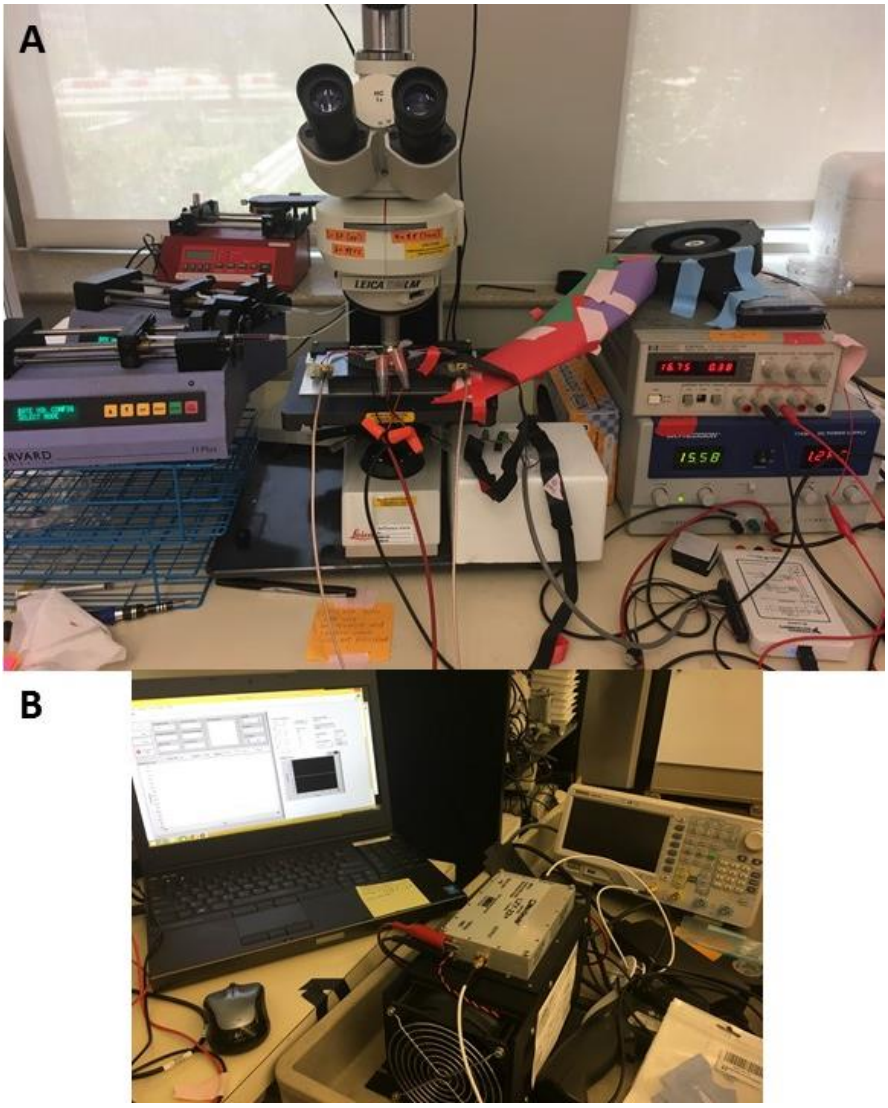

Fig. 21 Setup of the acoustic blood separation experiment with temperature regulation. A) Flow and temperature regulation equipment. B) Computer for PID control and driving electronics for the transducer.

The amount of bare wire around the transducer setup made it susceptible to radio frequency noise and possible coupling. During initial experiments, shifts in the temperature on one or both probes were seen when power was applied and withdrawn from the transducer (Fig.

22). Ferrites compatible with the frequency range used here were added to the coaxial cables and seen to reduce the shift in temperature from several degrees to <0.2°C. The noise was found to originate from the coaxial cables and power amplifier, potentially affecting the wires near the DAQ, as opposed to at the location of the transducer. Coaxial cables were wrapped 6-7 times through the ferrites.

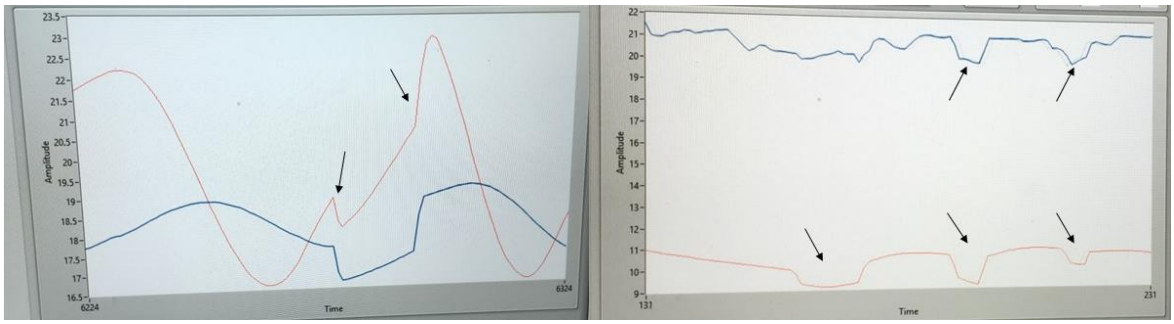

Fig. 22 Shifts in the temperature data were seen to be caused by noise from the coaxial cables and/or power amplifier. Adding ferrites to the coaxial cables reduced the fluctuation of the temperature signal to <0.2°C.

2.4 Blood Separation

Whole bovine blood with CPDA-1 anticoagulant was obtained from Texas A&M University Veterinary Medicine and Biomedical Sciences. The blood was used within several days of being drawn and ideally within the same day. Depending on the blood sample age,

behavior of the blood in the PDMS channel varied, even clotting or creating a stenosis. Therefore, fresh blood is the best choice for this system.

To perform a blood separation experiment, the transducer was first mounted onto the microscope stage and taped down. Coaxial cables connected the power amplifier and transducer, using a coaxial T-junction for SSAW transducers, in order to power both sides with approximately the same signal. The function generator was turned on and set to the transducer resonant frequency. A microfluidic channel was cleaned with IPA, dried with compressed air, and brought into contact with the transducer surface, attempting to align the channel alignment markers with those of the transducer. PBS was prepared and 1 mL syringe was loaded with several hundred microliters. The syringe was up-ended and air bubbles removed. Similarly, another syringe was loaded with whole blood. Each syringe was loaded into a separate syringe pump and the pump was turned on until fluid was seen to flow out of the needle. The tubing of the microchannel was connected to the two syringes with the blood syringe being connected to the central inlet of the trifurcated channel. The fluids were pumped down the tubing at 10 μL/min and the microscope was focused on the channel inlet trifurcation. Once the fluids arrived at the channel inlets, the flow rate for the blood was reduced to 3 μL/min. To remove any air bubbles or initial channel clogging at the entrance of exit, the syringe was manually depressed by a small amount. Once three laminar streams were formed as prescribed earlier, acoustic experiments began. The power amplifier was turned on and input voltage was varied to find the necessary voltage to create sorting of the blood cells. Initially, voltage above 300 mV_{pp} was used to determine if the channel was aligned with the standing wave nodes. If not, the power was turned off and the microchannel was repositioned on the substrate. This process was repeated until two nodes were seen by each channel wall along the length of the channel. If the channel was

properly aligned, clear fluid would exit the central outlet on the microscope image when the applied voltage was high enough. Finally, variations of input parameters for the blood separation, such as flow rate, voltage, and frequency, were varied and tested. To perform a temperature-regulated experiment, the temperature regulation system was mounted on the stage with the transducer, the thermocouple placed behind one of the electrodes, and the software used to cool the transducer to 18°C. The fan was positioned such that most of the air flowed through the heat sink and was taped into position. The temperature was recorded throughout the experiment. Videos and images of the effect of the transducer on the sample were captured throughout.

2.5 Effect on Small Particles

In order to assess the net occurrence of diffusion, dispersion and transport of nanoparticles in the passive (laminar flow-only) and acoustic scenario, nanoparticle absorption under brightfield microscope was used as an indicator of the nanoparticle distribution. Figure 23 shows the ideal acoustic experiment (active) scenario. In the ideal passive scenario, there would be no diffusion of nanoparticles from the sample stream into the buffer stream. The scenarios were observed during the same experiment.

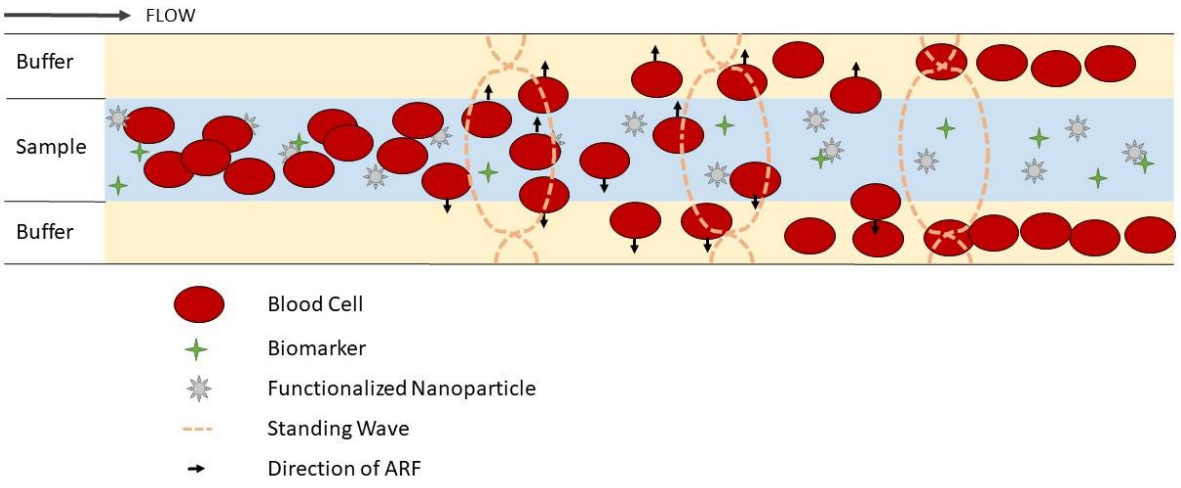

Fig. 23 In the ideal acoustic sorting scenario, nanoparticles and biomarkers remain in the plasma in the original streamline to be collected.

In the experiment, similar to the experimental procedure discussed in the Blood Separation section, a microfluidic channel coupled to the SAW transducer surface was flowed with whole blood in the central inlet and saline in the outer inlet. The channel was aligned such that the blood cells moved to sidewall positions along the length of the channel under acoustic influence. The channel was flushed with PBS followed by air to clear all blood cells and, then, nanoparticle-spiked plasma was pumped through the center inlet with PBS sheath pumped from the outer inlet. To make the nanoparticle solution, PEG-ylated gold nanoparticles obtained commercially (GNP-DYE-15-10-04-C3, Luna Nanotech Inc.) were diluted in blood plasma, yielding a final concentration of 61 nM. The nanoparticles were incubated with 1% BSA solution because the particles clumped together when suspended in plasma in initial tests, creating

micron-sized groups. BSA incubation is performed in order to prevent nonspecific protein interaction. Blood plasma was obtained by centrifuging whole blood for 10 minutes at 1300 rcf and aspirating the plasma. The nanoparticle-spiked plasma was flowed through the central inlet of the channel and PBS was flowed through the outer inlet. Flow rates were adjusted so that the plasma stream should exit the central outlet when neglecting diffusion effects. Flow rates of 3 and 10 μL/min were used for the nanoparticle solution and PBS, respectively, using the 11Plus pump. The distribution of the particles along the length of the main channel was observed via absorption under the microscope. To test the effect of acoustic influence, voltage from 200-500 mV_{pp} was applied and the distribution of the nanoparticle solution is observed. To observe any differences in behavior upon the introduction of blood cells, the channel was flushed with PBS and air and, then, whole blood diluted in nanoparticle-spiked plasma (1:10) was passed through the system and observed in the passive and active scenario.

CHAPTER III

RESULTS AND DISCUSSION

3.1 Surface Acoustic Wave Transducer

3.1.1 Fabrication

Fabrication results for different electrode metals are shown in Fig. 24. The single metal transducers, where only aluminum or gold was deposited, were prone to scratches and had poor adhesion to the substrate, resulting in electrode damage after a small number of experiments. Adding a chromium layer between the transducer surface and primary electrode metal showed improved performance and integrity as compared to single metal electrodes. Aluminum-containing electrodes produced electrodes with the smallest number of defects, whereas gold fabrications had a number of small and large defects. Surface and electrode defects could alter resonance and change transmission properties of the transducer. In the worst case, these defects and scratches resulted in an unusable transducer due to open circuit. The defects seen in the gold electrode fabrication are thought to be due to poor-quality of the gold used. Passivation of electrodes may be a useful step to prevent scratches; however, the process would require optimization to ensure a uniform layer and electric field.

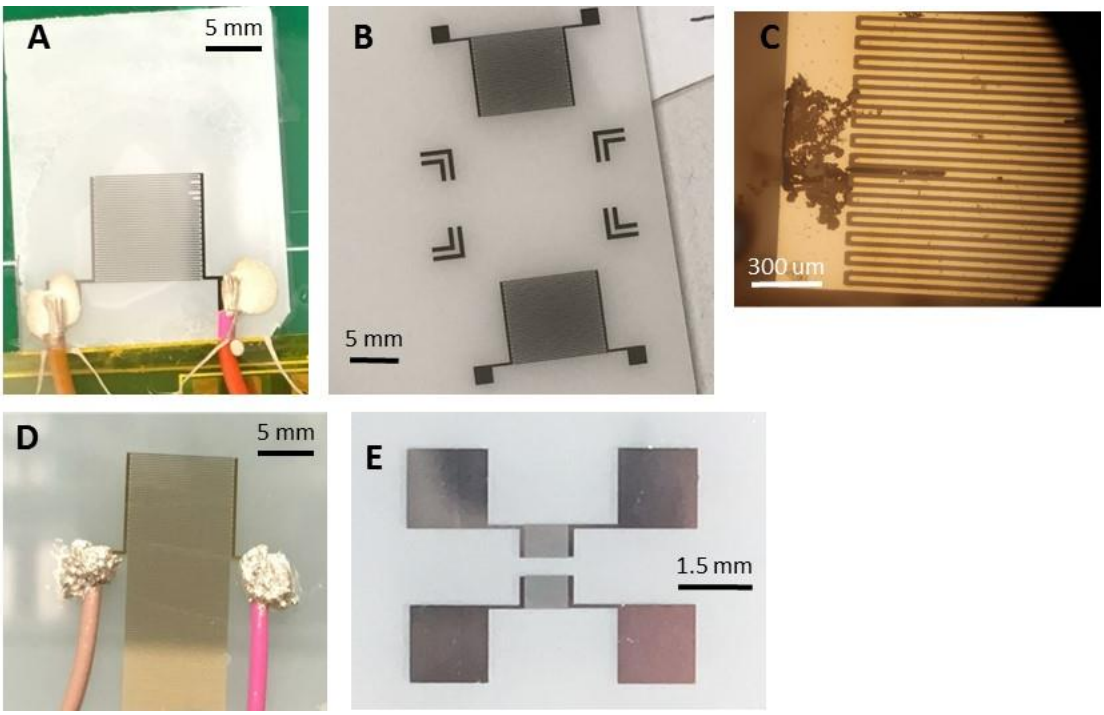

Fig. 24 Transducers fabricated with A,E) aluminum, B) chromium-aluminum, C) gold, and D) chromium-gold. The electrodes shown here have a design frequency of 7.54 MHz, except for E, which has a design frequency of ~90 MHz.

The first batches of transducers showed several issues during testing (Fig.25A-C). An amplitude of several volts input signal through the power amplifier resulted in electro-migration, the transport of excited ions in instances of high current and small structures. Cracking of the piezoelectric substrate was also observed frequently and was initiated by either pressure on the transducer surface or several volts of signal amplitude. It would appear that existing cracks were propagated by these triggers. For the SSAW chromium-aluminum transducers, scratches were already present from the fabrication process (Fig. 25D). However, the transducer showed

resonance near the design frequency and transmission similar to transducers with electrodes with no obvious defects.

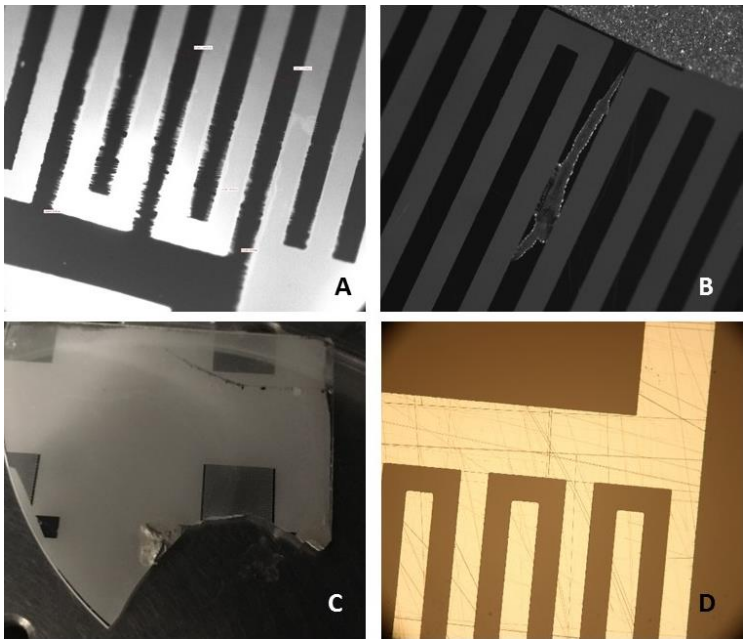

Fig. 25 Transducer failures observed during testing, including A,B) electro-migration, C) cracking, and D) scratches. A-C show aluminum electrode devices from the first several rounds of fabrication. Most of the scratches seen in D) were present from fabrication. However, similar scratches occurred due to cleaning of the transducer after testing.

3.1.2 Characterization

Successfully fabricated transducers were characterized with a network analyzer prior to testing. Fig. 26 shows the S11 of a low and high frequency TSAW device, with design frequencies of 7.54 MHz and ~90 MHz. The low frequency device is seen to have multiple

resonances. Those peaks away from the design resonance may be other types of resonances or may be due to the condition of the crystal. Testing at these other resonances showed low acoustic utility, inducing much smaller forces on plastic beads suspended in water. The high frequency device is seen to resonate only at one frequency, as the other peak is its harmonic. Resonance at harmonics is expected and is seen to have higher transmission properties.

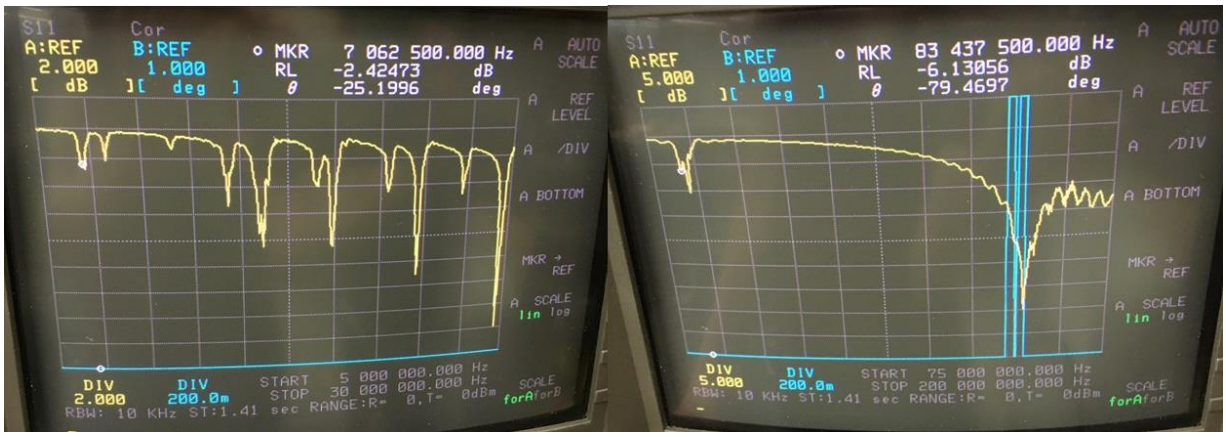

Fig. 26 S11 of low frequency (left) and high frequency (right) TSAW transducers. Low frequency devices had design resonance at 7.54 MHz and high frequency devices had design resonance at ~90 MHz. Insertion loss for the high frequency device was much higher than for low frequency devices. Low frequency devices were seen to have additional resonances apart from the design frequency.

S11 of both electrodes of a SSAW device over time is shown in Fig. 25. As can be seen, the resonance peak shifted over time (and use). Initially, transducer was driven unmatched at the resonance frequency. However, over time, the transmission appeared to decrease. Upon

measurement, the resonant frequency was observed to be shifted and the attenuation value was reduced. From fabrication, the highest initial attenuation value was ~2.5 dB for electrodes without defects (Fig. 27A). Testing appeared to decrease this value. Therefore, the SSAW transducers were matched to provide maximum transmission at the new resonant frequency and provide similar properties for the paired electrodes (Fig. 27B-D). SSAW transducer #4 was matched approximately once a month.

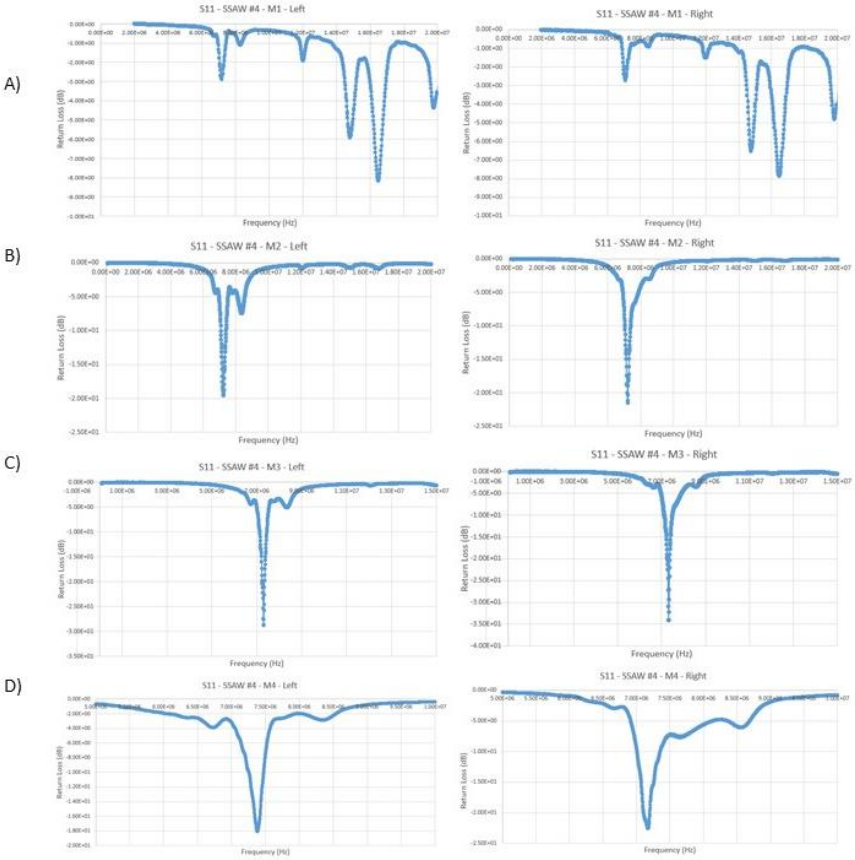

Fig. 27 S11 of SSAW transducer #4 over time, showing results for the left electrode in the left column and right electrode in the right column. A) S11 of the unmatched transducer directly following fabrication. The attenuation value was ~-2.5 dB. (B-D) The transducer was matched after experiments showed decreased performance. Matching the transducer yielded attenuation values of -20 to -35 dB.

TSAW transducer function was tested with simple droplet mixing experiments to determine effect of frequency and initial power requirement. The sample was polystyrene beads suspended in water and, due to the asymmetry of the droplet, significant ASF is generated when the transducer is turned on. Low frequency devices (7.05 MHz) showed moderate streaming forces that produced mixing and some aggregation of beads into several clumps. Using a slightly higher frequency (20.4 MHz) showed much faster mixing and displayed clear, maintained vortices. Fig. 28 shows mixing of beads using 7.05 MHz and 20.4 MHz input. A significant voltage input was used in the experiment to observe the phenomenon. It can be seen that the number and location of vortices in the droplet varied between the two frequencies shown. Multiple mixing regimes are known to be produced depending on the experiment parameters (12). Each regime gives a unique result with a different streaming pattern and overall effect. Using a high frequency device actuated at its resonance yielded centrifugation of plastic beads (Fig. 29). The beads are seen collected together after the transducer is turned off (Fig. 29C). This device required a much lower voltage input to produce a significant effect. This was expected because higher frequencies are higher energy waves; thus, the amplitude can be lower.

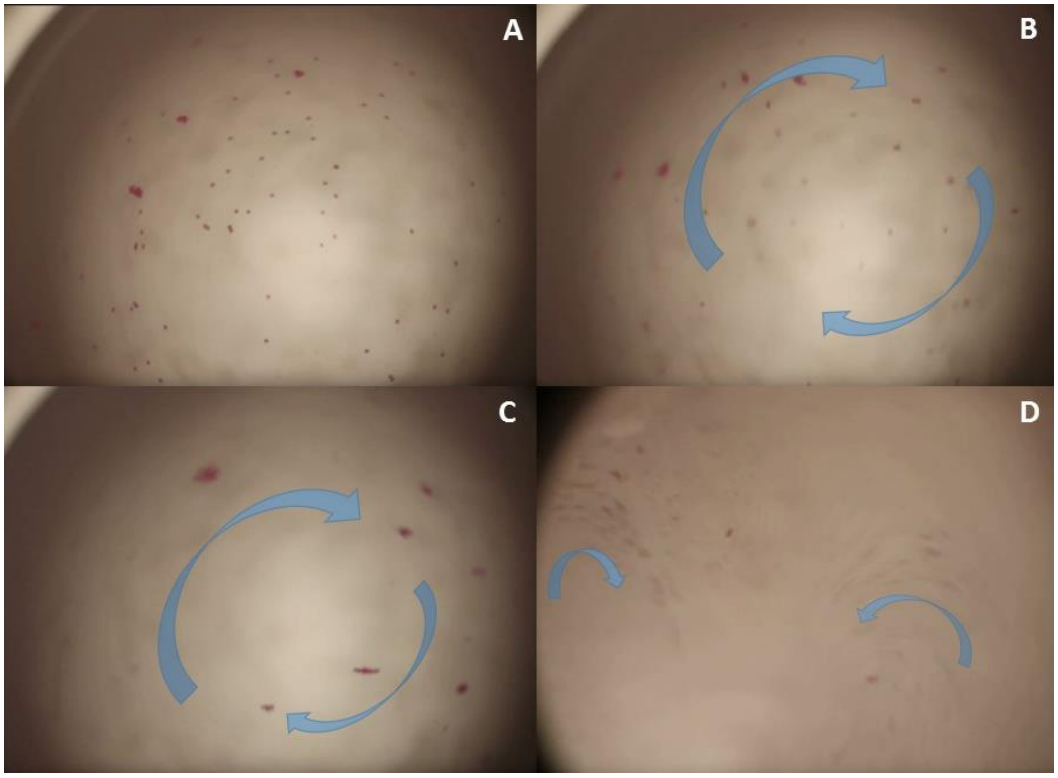

Fig. 28 Centrifugation experiments to test TSAW transducer function and frequency. (A-C) show centrifugation at 7.05 MHz with input voltage of 450 mV_{pp} at 0 seconds (A), 1 second (B), and 36 seconds. Mixing with moderate velocity is observed. The effect strengthened over time. D) shows two vortices generated by a low frequency TSAW transducer actuated at 20.4 MHz and 450 mV_{pp}. Mixing velocity was increased as compared to the experiments at 7.05 MHz. Different experiment parameters may produce varied vortices patterns as shown here.

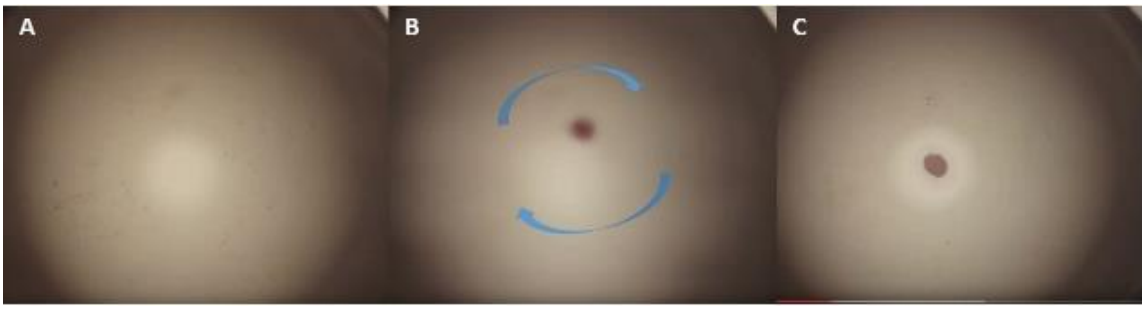

Fig. 29 Acoustic streaming experiment using high frequency TSAW device actuated at 83.75 MHz and 250 mV_{pp} input at 0 seconds (A), 4 seconds (B), and 17 seconds (C). Use of higher frequency resulted in increased streaming forces and effective concentration of polystyrene beads.

SSAW transducers were driven at resonance at multiple voltage levels to observe heat generation per voltage input with an infrared camera. Fig. 30 shows the heating for SSAW device #1 which, at the time of the experiment, had been used in numerous blood separation experiments and had a matching circuit. The average temperature at the location of the bulls-eye is displayed in the upper left corner of the images and the scale is located at the bottom of the images. Heating was significant for voltage inputs that were used for effective blood separation in the detachable platform. Fig. 31 shows heat generation for SSAW #4, which had not been used in blood separation tests and was unmatched at the time of this experiment. The heat generation for this device at resonance and the same voltage inputs is seen to be less. It would appear that more heating occurs over transducer use and changes in the properties of the piezoelectric substrate or electrodes may be the reason. As the transducer was used in a greater number of experiments, the transducer temperature was found to be more difficult to regulate and the transducer performance in the blood separation experiment declined. Potential reasons

for changes to the transducer properties are discussed further in the Blood Separation results section. These measurements were also taken with the microfluidic channel placed between the electrodes. However, no significant differences were observed.

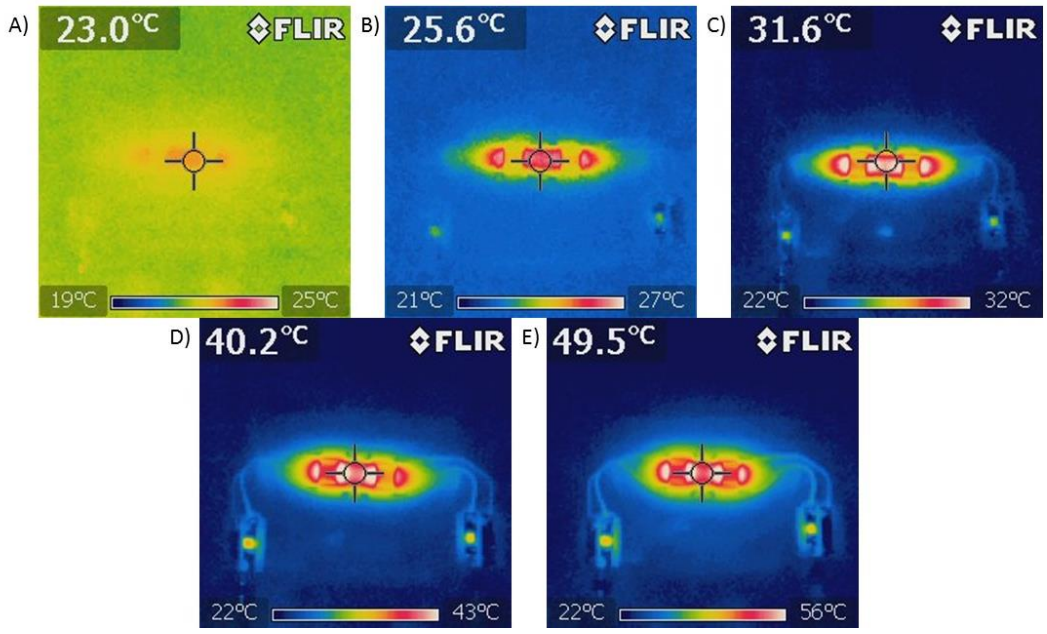

Fig. 30 Infrared temperature measurement of SSAW transducer #1. SSAW transducer #1 had been used in multiple blood separation experiments prior to this measurement. Images show the temperature at the location of the bulls-eye (and hot spot) after 60 seconds of resonant input at A) 100 mV_{pp}, B) 200 mV_{pp}, C) 300 mV_{pp}, D) 400 mV_{pp}, and E) 500 mV_{pp}. Significant heat is generated at higher voltages which were more commonly used in blood separation experiments.

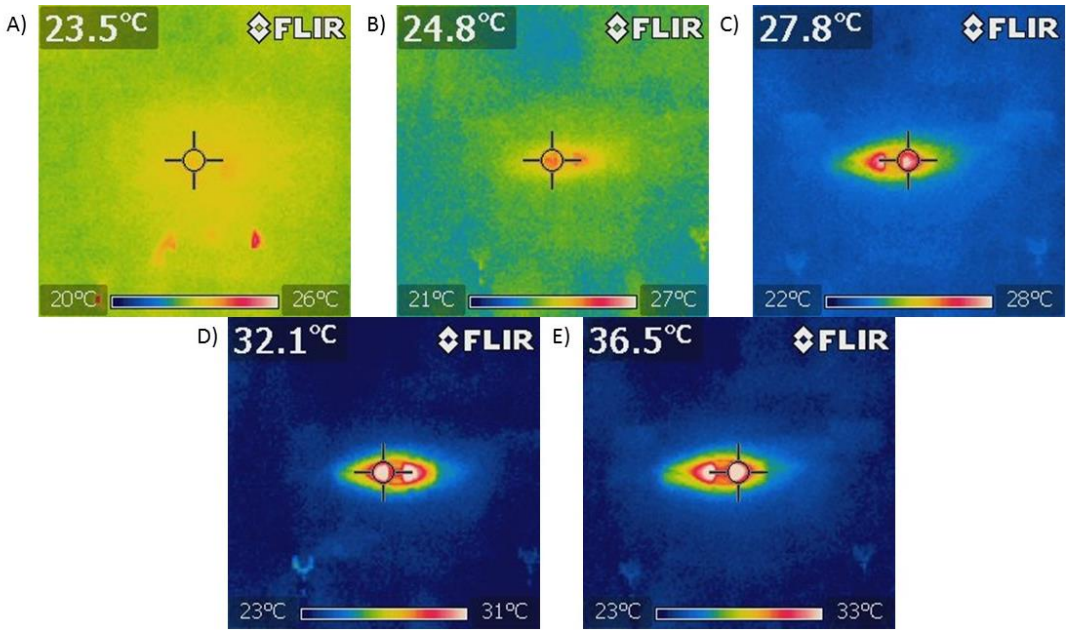

Fig. 31 Infrared temperature measurement of SSAW transducer #4 which had not been used prior to collection of this data. Images show the temperature at the location of the bulls-eye (and hot spot) after 60 seconds of resonant input at A) 100 mV_{pp}, B) 200 mV_{pp}, C) 300 mV_{pp}, D) 400 mV_{pp}, and E) 500 mV_{pp}. The temperature increase per voltage input is seen to be reduced compared with the temperature change seen with SSAW transducer #1.

3.2 Microfluidic Channel

3.2.1 Fabrication

Examples of fabricated glass-PDMS and PDMS-PDMS channels for acoustic experiments are shown in Fig. 32. Although the bonding protocols were optimized, the channel had to be checked throughout experiments to confirm there was no leaking. Manually driving the syringes sometimes led to cracks and tears in the cover glass and thin PDMS layers.

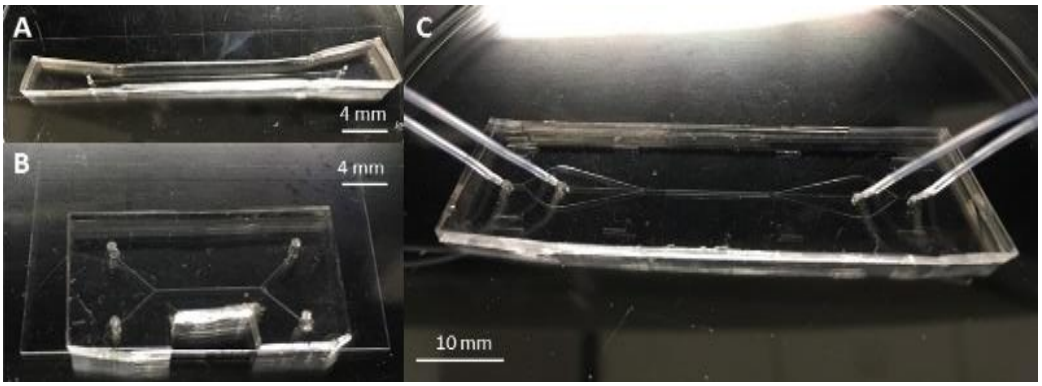

Fig. 32 Fabricated glass-PDMS (A,B) and PDMS-PDMS (C) microfluidic devices for TSAW (A,B) and SSAW (C) experiments.

3.2.2 Characterization

Setup of laminar streams in a trifurcated microfluidic channel with a 15 mm main channel length is shown in Fig. 33. Flow rates were selected such that acoustic sorting resulted in high clarity of the central stream fluid at the lowest voltage necessary. Clarity is defined by the color and cell content relative to PBS in the microchannel, and, thus, also as a lack of red pigment, which red blood cells display at significant concentrations. Red coloration of solutions containing red blood cells was visible above and below 4% cell volume in a sample. A small number of cells in solution could be visualized as dark spots in the solution. 3 and 10 μL/min were selected as the best flow rates for the SSAW experiments using the Harvard apparatus 11Plus pumps (Fig. 33). The channel length chosen for the final blood separation experiment was 15 mm from trifurcation to trifurcation to limit diffusion. Using these flow rates with the final flow system, 25 μL of whole blood can be processed in 27 minutes, where 25 μL is the plasma volume used to measure biomarker concentration with the optical nanoparticle-based assays

mentioned in Chapter I. The 11Plus pumps used in this experiment were not particularly stable at the low end of its range (0-5 μL/min). At lower flow rates and larger ratios, pulsation was common. Pulsation may be caused by the pump mechanism, by a buildup of pressure in the high density blood sample, or due a large difference in velocity between the laminar streams, which was seen using a large ratio of flow rates between sample and buffer.

Fig. 33 Example of flow set up for acoustic experiment, showing the entrance (left) and exit (right) of the microfluidic channel with the transducer off. Undiluted whole blood is placed in the central stream and sheathed by two PBS streams. Flow rates of 3 and 10 μL/min were used for blood and PBS, respectively. The channel length selected for final blood separation experiments was 15 mm between the two junctions. No significant diffusion of blood cells was observed. The main channel width and height were 150 μm and 50 um, respectively.

Flow rates of 0.25 and 5 μL/min for blood and PBS, respectively, were tested using the Harvard Apparatus PHD ULTRA pump, which had a lower flow rate capability compared with

the 11Plus. Fig. 34 shows the control laminar flow in a microchannel with 25 mm main channel length using these lower flow rates. These flow rates are the same as reported by Nam et al. (16) and, as mentioned in the blood separation section, yielded high clarity fluid in the center outlet stream. Using these flow rates, it would take one hour and forty minutes to process 25 μL of plasma. As can be seen, the diffusion of blood into the neighboring PBS streams is significant. This result may be caused by the lower flow rates used and/or the increased channel length when comparing to the experiment in Fig. 33. Fig. 34 is an example of how the channel length and flow rate parameters need to be balanced in the design of a final platform. Due to the manipulation and performance of the 11Plus pump discussed previously, without inserting flow rate monitors, a direct comparison between the flow rates and channel lengths used in Fig. 33 and Fig. 34 cannot be made.

Fig. 34 Laminar streams of blood and PBS shown at the exit trifurcation of a 25 mm long channel with flow rates of 0.25 and 5 μL/min for blood and PBS, respectively. Undiluted whole blood is placed in the central stream and sheathed by two PBS streams. Significant diffusion of blood cells was observed due to reduced flow rates and increased channel length compared with the experiment shown in Fig. 33. The main channel width was 150 um. The pillar structure width was 600 um.

One inlet, one outlet channel designs were used with a TSAW transducer to test the two detachable channel designs for their use in acoustic experiments, in order to eliminate other experiment factors such as alignment of the transducer and channel and flow changes due to channel geometry or clogging. Blood was used as the particles as blood was easier to suspend for durations of time compared with polystyrene particles. The blood was diluted 10X so that any acoustic forces acting on the blood cells could be visualized and the distribution of cells seen more clearly. Fig. 35 shows the result of unidirectional ARF at different voltage levels on a

diluted blood sample where the TSAW transducer is located to the top of the image. It can be seen that the power required for the glass-PDMS channel was greater to achieve similar displacement of cells as compared to the PDMS-PDMS channel. Using the glass-PDMS channel, at 150 mV_{pp}, there is no significant displacement of cells. At 400 mV_{pp}, a portion of the blood cells are displaced to the far wall (bottom of the image). However, a portion of the cells also is caught in the central flow stream. The ARF is not large enough to drive these cells and those near the top wall toward the far wall. Using the PDMS-PDMS channel, 150 mV_{pp} input results in an ARF that causes a band of red blood cells to form and be displaced over the acoustic aperture (as the cells move along the channel). Using 400 mV_{pp}, a greater portion of the red blood cells are displaced. In this case, blood cells remain by the channel wall near to the electrode also. The PDMS-PDMS channel design was selected for blood separation experiments due to its lower power requirement and repeatability. This result shows that the ARF is not large enough to overcome the forces at the wall. Therefore, it is prudent to place the blood sample away from the walls in order to increase the percent separation achieved in sorting. Based on this, a trifurcated microchannel was designed and used for blood separation experiments with the sample placed in the middle stream away from channel walls.

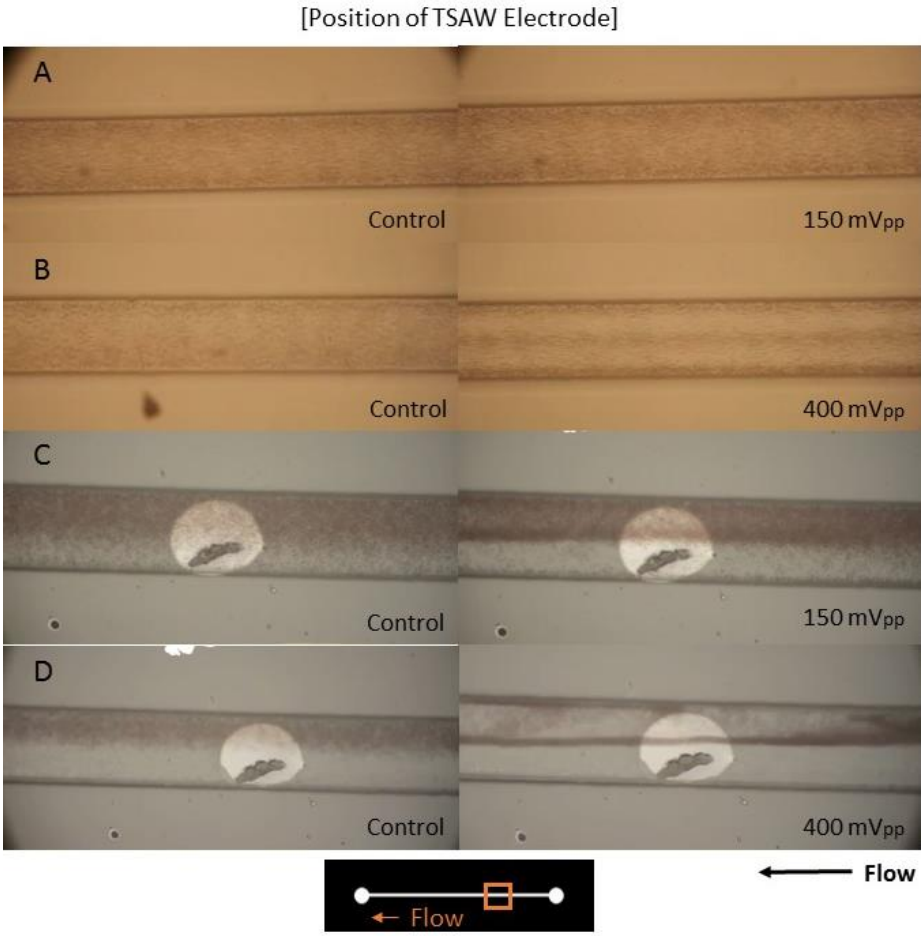

Fig. 35 TSAW transducers were used to test displacement of 10X diluted blood at 150 mV_{pp} and 400 mV_{pp} using a PDMS-glass channel (A,B) and PDMS-PDMS channel (C,D) with single inlet, single outlet channel design. Using the glass-PDMS channel, displacement at 150 mV_{pp} was not significant. A portion of blood cells were displaced at 400 mV_{pp}, but the ARF was not large enough to effect the majority of cells. Using the PDMS-PDMS channel, displacement at 150 mV_{pp} was significant; a dark band of cells is seen to form in the microchannel away from the TSAW electrode but a large portion remained near the channel wall. At 400 mV_{pp}, the majority of cells are displaced significantly away from the channel wall with greater displacement as cells move farther through the acoustic aperture. A reduced fraction of blood cells remained at the walls. The PDMS-PDMS channel design was selected for blood separation experiments due to its lower power requirement and repeatability.

3.3 Integrated System

Due to requirements of 25-30 μL of plasma to carry out a nanoparticle-based assay, the transducer and blood separation performance needed to be maintained for at least 30 minutes. Heating of the transducer caused blood separation performance to decline after several minutes due to temperature-dependent properties of the transducer. Therefore, a cooling system was built, using a Peltier element, thermocouple, and PID feedback loop. The performance of the cooling system was tested by measuring the transducer temperature with and without the cooling system (Fig. 36). In addition, the temperature range using the cooling system is shown for experiments exhibiting high and low performance blood separation, where low separation refers to a significant reduction in clarity of the fluid exiting the center outlet of the channel either for the experiment duration or over time. With the addition of the cooling system, the temperature was controlled, although it plateaued above the set point (18°C). The transducer temperature was seen to plateau over time with the cooling system for both high and low performance blood separation experiments. When the transducer produced high performance blood separation, temperature was maintained at a value between 20-27°C (shown by the dashed lines in Fig. 36). If the system can either be cooled to the set point temperature or plateaus at a temperature less than 27°C, the cooling system built here can be used to facilitate long-term cell sorting experiments. After using the transducer for several weeks, blood separation performance declined and, in some experiments, the heat produced was increased. Changes to the transducer properties, including heat produced from the piezoelectric conversion process, were hypothesized to have occurred due to damage of the SAW electrodes or the substrate. Changes may occur due to scratches or micro-cracks which can cause the resonance of the device to shift and may be exacerbated by use of high voltage and high frequency (54), which are employed

here. The blue and gray curves in Fig. 36 show the temperature of the transducer with and without the cooling system after blood separation performance decline. Without the cooling system, the temperature of the transducer continued to rise. With the cooling system, the increased heating of the transducer could be controlled although at a higher value than where high performance blood separation was seen to be commonly achieved. Therefore, if the transducer were used for a time after the performance declined, a cooling system with greater cooling capability would be required.

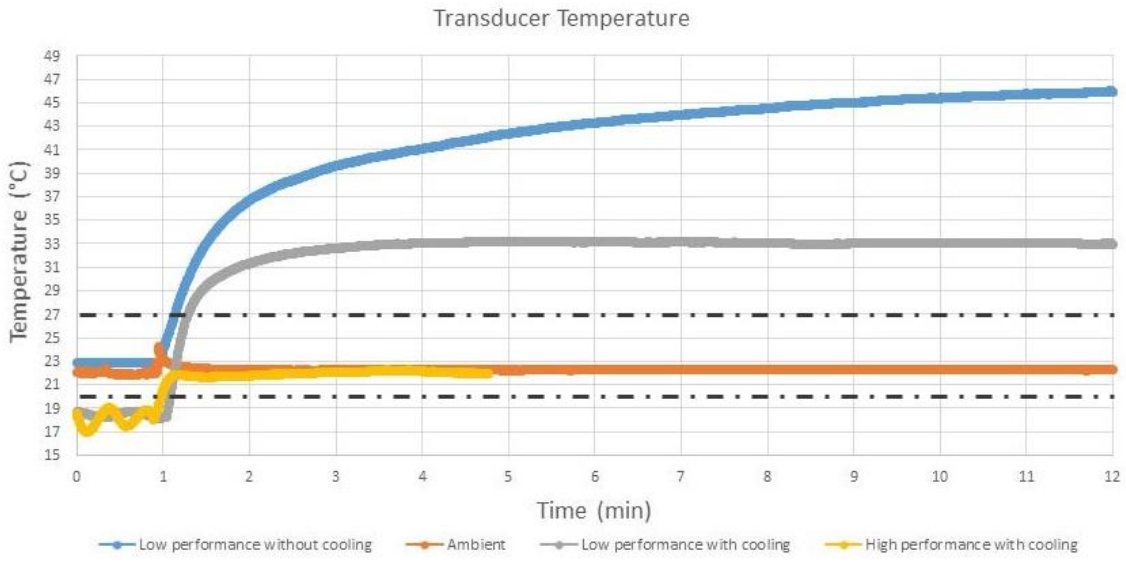

Fig. 36 With the addition of the cooling system, the transducer temperature was controlled, although it plateaued above the set point. Yellow and gray curves are examples of how the transducer temperature could be controlled with the cooling system. The blue curve shows that the transducer temperature continued to rise over time without use of the cooling system. The dashed lines indicate the temperature range where high performance blood separation was achieved and maintained. After using a transducer for several weeks, blood separation performance declined and in some experiments the heat produced increased. The gray and blue curves shows the transducer temperature with and without the cooling system when the blood separation was not maintained and had reduced performance from previous experiments. The orange curve represents the room temperature.

The Peltier element used here was able to cool the transducer during the first few weeks of transducer use. For voltage levels between 300-550 mV_{pp}, transducer temperature was maintained at temperatures between 19-29°C. As mentioned above, blood was sorted in these experiments, producing what appeared visually to be high percent separation with clear fluid in the center outlet. There were a few instances where the transducer unexpectedly seemed to over-heat and caused the heat sink to saturate and heat to flow back toward the transducer. After about four to six weeks of use, for both SSAW transducer #1 and #4, the transducer was not able to be cooled such that blood separation performance was sustained and the center outlet contained clear fluid. While, at this point, the transducers were sometimes cooled to 26-30°C, the blood separation experiment resulted in blood separation below previous performance, either producing what appeared to be reduced percent separation (where nodes are still visible) or simply dispersed cells (where nodes were not visible), despite increases in voltage or adjusting the resonant frequency, after the temperature had plateaued. This is hypothesized to be due to changes in the transmission properties of the transducer, possibly due to damage. Therefore, in the practical application of this platform for diagnostics, it may be required to replace the transducer every day or every few days based on the throughput required to process one sample and the assumption of using the transducer to process multiple patient samples each day.

Although blood separation performance declined, likely due to changes in the transducer, the cooling system was found to facilitate longer sorting experiments. Fig. 37 shows a blood separation experiment over the course of 30 minutes, using a cooled SSAW transducer with degraded performance. The transducer was driven at resonance with a voltage of 450 mV_{pp}. Temperature was maintained between 25-27°C. Flow rate was 3 and 10 μL/min for the sample and buffer, respectively. It can be seen that the visual extent of separation, migration of blood

cells to the nodal positions at the wall, was similar from 0 minutes throughout the experiment to 32 minutes. Therefore, the cooling system built here was seen to be capable of maintaining transducer temperature for long-term experiments and facilitating consistent blood separation performance.

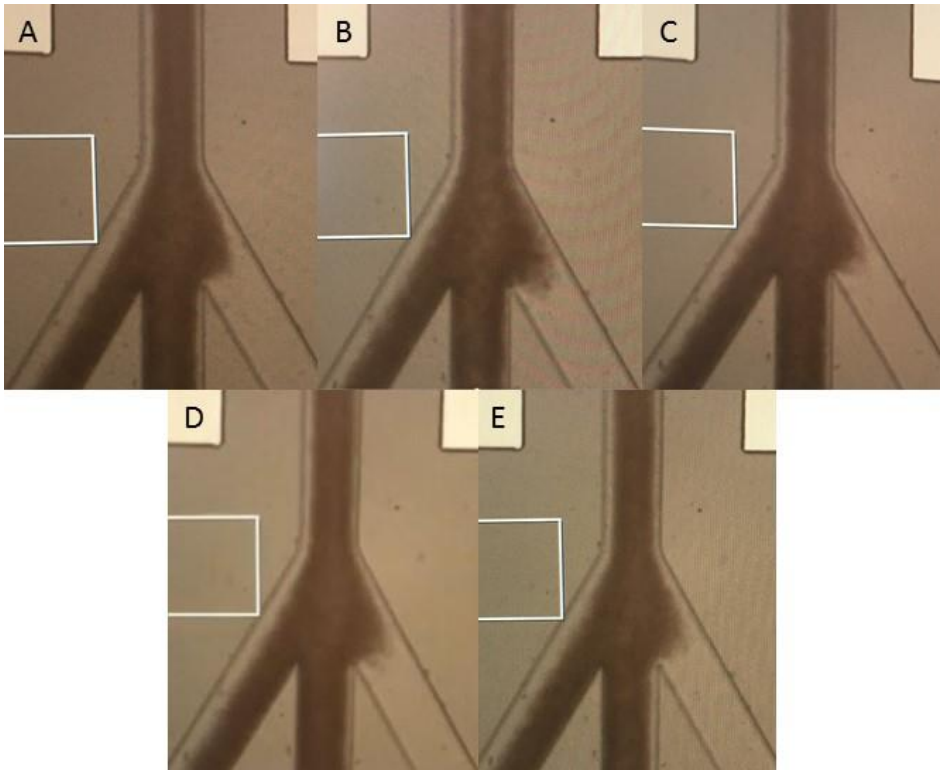

Fig. 37 Blood separation using a SSAW transducer with degraded performance at 0 minutes (A), 8 minutes (B), 23 minutes (C), 28 minutes (D), and 32 minutes (E). Migration of blood cells to the nodal positions at the wall, was similar from 0 minutes throughout the experiment to 32 minutes, showing that the temperature regulation system was able to maintain transducer temperature for at least 30 minutes. Input voltage was 450 mV_{pp} and transducer temperature was 25-27°C throughout. Flow rates of the sample and buffer were 3 and 10 µL/min. Note that the bottom right outlet branch was clogged during this experiment.

3.4 Blood Separation

3.4.1 Blood Separation using TSAW

TSAW can potentially be implemented for blood separation and offers benefits of reducing the amount of piezoelectric substrate required and increasing the achievable displacement of particles. Fig. 38 shows blood cells being deflected from the wall near the electrode into the PBS stream and toward the other side of the channel. The cells are displaced farther transversely as they continue to be exposed to ARF as they flow through the acoustic aperture. However, only a portion of the cells are deflected with the remaining cells unmoved due to forces at the channel wall. The flow rates were 0.2 and 2 μL/min for blood and PBS, respectively, using the 11Plus pump. Applied voltage was 450 mV_{pp}. Since we desire to separate whole blood to extract high purity plasma, TSAW does not appear to be a good design choice. However, use of sheath flow on both sides of the sample and TSAW sorting may yield a different result. The channel design was switched to a trifurcated design to position the blood sample in the center stream for more efficient sorting.

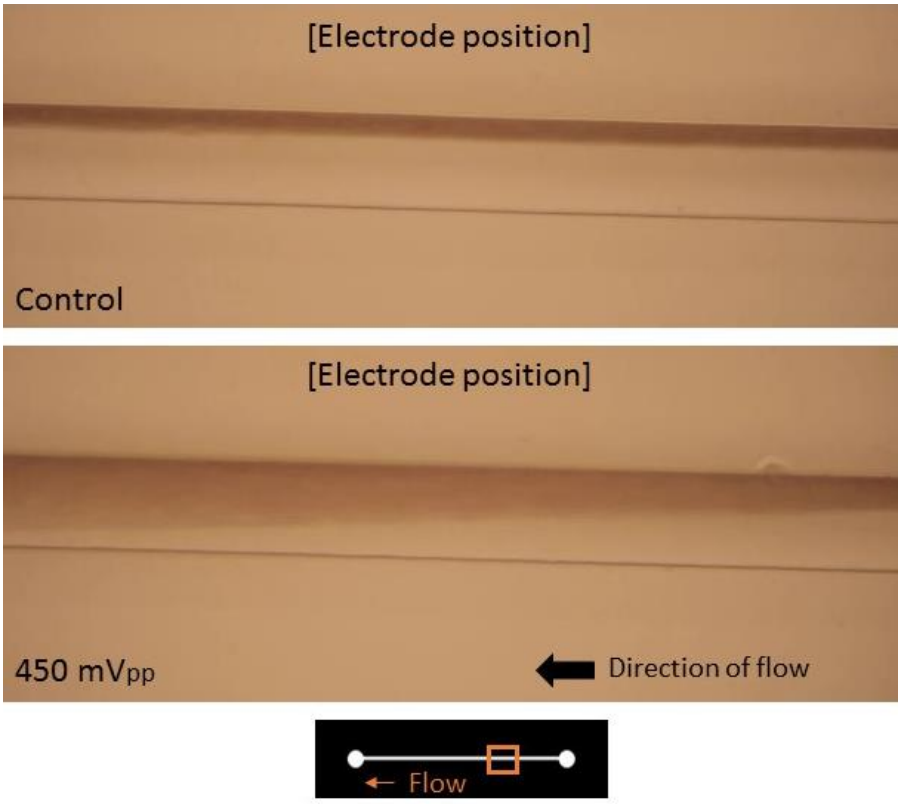

Fig. 38 TSAW-based whole blood separation. The cells are displaced farther transversely with continued exposure to the ARF as they flow through the acoustic aperture. However, only a portion of the cells are deflected with the remaining cells unmoved due to forces at the channel wall. Images were taken where the beginning of the transducer aperture aligned with the channel. The location is approximately shown by the orange box on the photomask image. The flow rates were 0.2 and 2 µL/min for blood and PBS, respectively. Applied voltage was 450 mV_{pp}.

3.4.2 Blood Separation using SSAW

Using SSAW transducers and a trifurcated PDMS pillar channel, undiluted whole blood separation was achieved. Fig. 39 shows images of the channel outlet trifurcation over time as the transducer is turned on. Flow rates for the experiment shown in the figure were 0.25 and 5 µL/min for the sample and sheath fluid, respectively, using the PHD ULTRA pump. Due to the

low flow rate and main channel length of 25 mm, diffusion was much larger prior to the transducer being turned on compared with the final channel selected, which has a channel length of 15 mm. Applied voltage was 550 mV_{pp}. Prior to the experiment, laminar streams are formed and the channel is aligned with the nodes of the standing wave. The channel was moved manually across the SAW substrate, actuating the transducer, until blood cells were seen to move to locations near the two sidewalls of the channel. Based on the theory, when this is achieved, the zero pressure nodes are located at the sidewalls and the ARF generated by the standing wave drives the blood cells toward the nodes due to their acoustic contrast and with larger force than smaller sample components. When the transducer was turned on to observe the quality of blood separation, ARF is seen to act on the blood cells, displacing the cells to the zero pressure nodes at the sidewalls. After several seconds, clear fluid was seen in the center stream near the channel exit. The percent removal appeared to be greater than 90%.

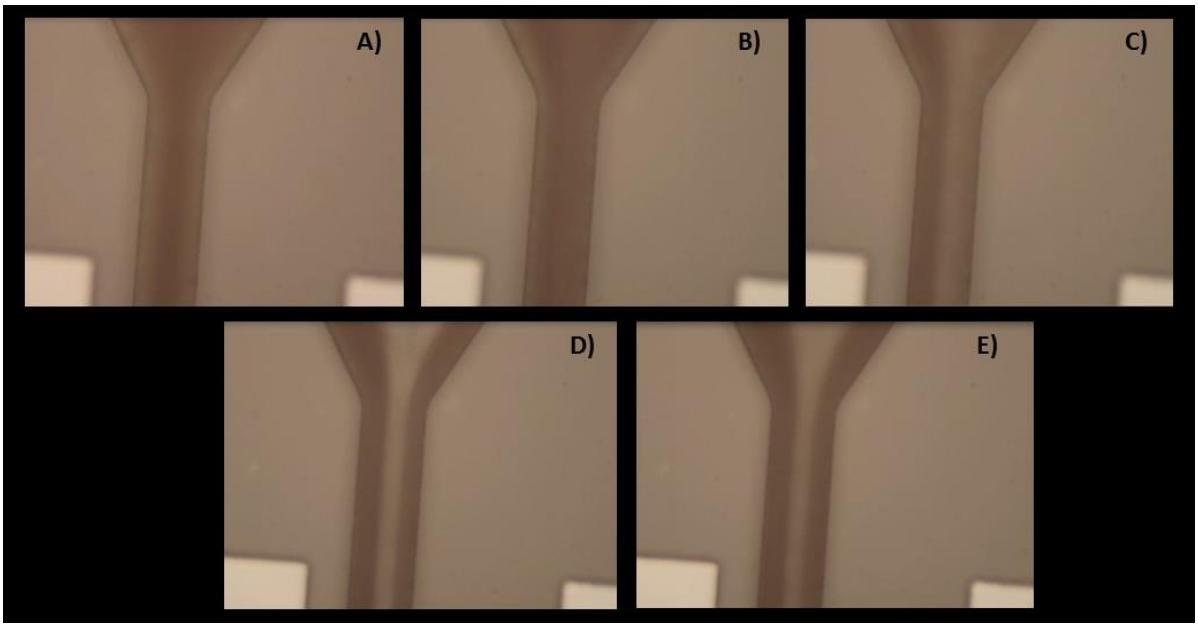

Fig. 39 Using SSAW transducers and a trifurcated PDMS pillar channel, high performance undiluted whole blood separation was achieved. Blood separation is shown at 0 seconds (A), 2 seconds (B), 5 seconds (C), 10 seconds (D), and 15 seconds (E). The input voltage was 550 mV_{pp}. Flow rate of the sample and buffer were 0.25 and 5 μL/min, respectively. Low flow rates and the use of a 25 mm main channel length resulted in significant diffusion between laminar streams before the transducer was turned on, as compared with the final channel length selected and other flow rates used.

Blood separation was achieved but not long term due to heating of the transducer. Piezoelectric transducers have transmission properties sensitive to changes in temperature and loading. Heating of the transducer substrate and, subsequently, the sample may cause changes in the sample speed of sound and electrode resistance, resulting in changes in resonance and transmission. Assays usually require 25-30 μL of plasma. This system requires about 30 minutes to process that volume when using flow rates of 3 and 10 μL/min for sample and sheath fluid, respectively. To make the system work for experiments longer than a few minutes, the

temperature was stabilized. Fig. 40 shows examples of undiluted whole blood separation achieved using the temperature regulation system. The location of both images is near the channel exit after the pillar structure, where the pressure waves propagate. Fig. 40A shows blood separation achieved at 380 mV_{pp} input with flow rates of 3 and 8 μL/min for the blood and sheath fluid, respectively, using the 11Plus pump. These settings yielded "high performance" blood separation based on the clarity of fluid in the central outlet. Fig. 40B shows blood separation achieved using 550 mV_{pp} voltage input and flow rates of 4 and 12 μL/min for the sample and sheath fluid, respectively. The reduced clarity of the center outlet fluid in Fig. 40B is likely due to use of temperature regulation system settings that were not optimized at the time of the experiment. The temperature during the experiment was held at 29°C, which was later found to be sub-optimal for system performance. In addition, these experiment using flow rates of approximately 3 and 10 μL/min may have been susceptible to flow disturbances from the instability of the pump used at lower flow rates. Similar separation to that shown in Fig. 39 should be achievable at slightly increased flow rates by using a pump with a lower flow rate capability and stability.

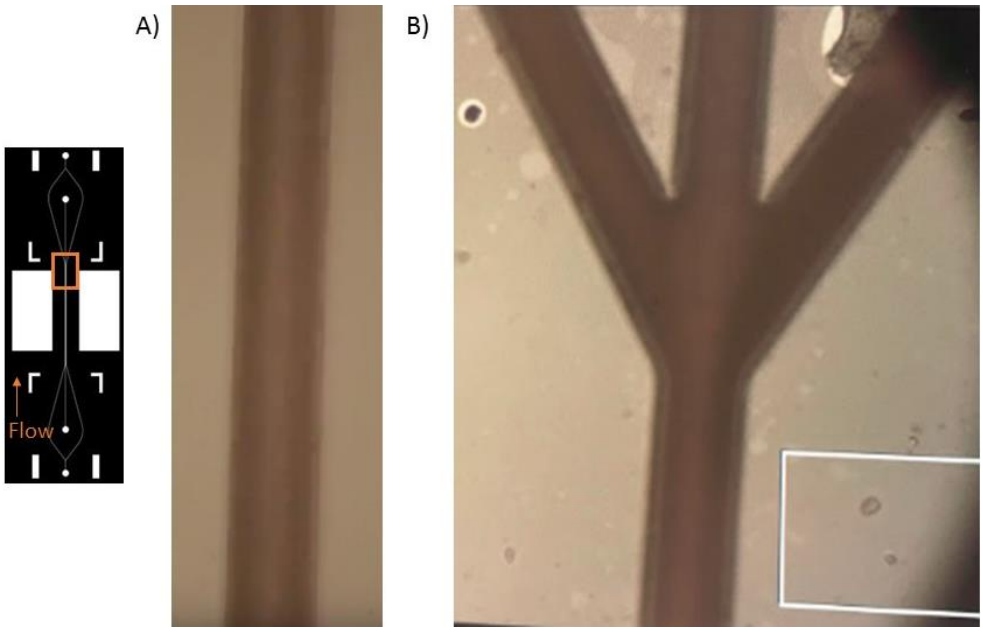

Fig. 40. Undiluted whole blood separation using the temperature regulation system and increased flow rates. A) Input voltage was 380 mV_{pp}. Flow rate of the sample and buffer were 3 and 8 µL/min. Transducer temperature was 19°C. These settings yielded high performance blood separation based on the clarity of fluid in the central outlet. B) Input voltage was 500 mV_{pp}. Flow rate of the sample and buffer were 4 and 12 µL/min. Transducer temperature was 29°C. The reduced clarity of the center outlet fluid is likely due to use of temperature regulation system settings that were not optimized at the time of the experiment. The boxed area of the black and white channel photomask (left) indicates the approximate location imaged.

The microfluidic channel used in the previous figures had 150 µm branch width at the trifurcation, which leads to some degradation of the sorting at the trifurcation due to changing flow rate. The cell distribution across the outlet branches using the channel with 50 µm branch width (and 150 µm main channel width) was much improved as compared to these experiments; however, experiments using channels with 50 µm branch width had temperature stability issues, discussed below, due to changes in the transducer properties. While, in the case of this

experiment, the system temperature was able to be controlled, the transducer performance was less than it had been in the weeks preceding the experiment.

For most blood separation experiments performed, a significant percentage of blood cells could be seen at the two nodal positions at temperatures up to 29°C. As shown in Fig. 36 in the integration section, using the cooling system, blood separation sustained with similar clarity over time was produced when the transducer temperature was maintained between 20-27°C. Therefore, if transducers can be maintained at a temperature in this range, this system may produce high percent separation of whole blood for experiments longer than several minutes. One challenge for quantification is redesign of the channel outlet-tubing junctions. The current designs results in a reduction of flow rate at the junction between microfluidic channel and tubing causing mixing and diffusion between blood present from when the transducer was off and also with any blood cells sedimented at the junction with clear fluid from when the transducer is on. These junctions were fabricated at an angle to help reduce issues but require further re-design to provide optimal plasma collection.

3.4.3 Transducer Performance over Time

Short-term changes in transducer performance were observed within experiments. Fig. 36 shows a SSAW blood separation experiment performed with the temperature regulation system. In this experiment, over the course of 30 seconds, the temperature increased by 10°C resulting in the sorting effect fading quickly. This fading effect was observed with multiple transducers with and without temperature regulation. In other similar experiments, cells were displaced to the nodes near the channel wall immediately after the transducer was turned on, but, over the course of 5-30 seconds, the sorting effect completely faded and the sample returned to the control flow

scenario. The most likely cause of this short-term effect is transducer heating. Resonance frequency and transmission properties of acoustic transducers are dependent on temperature.

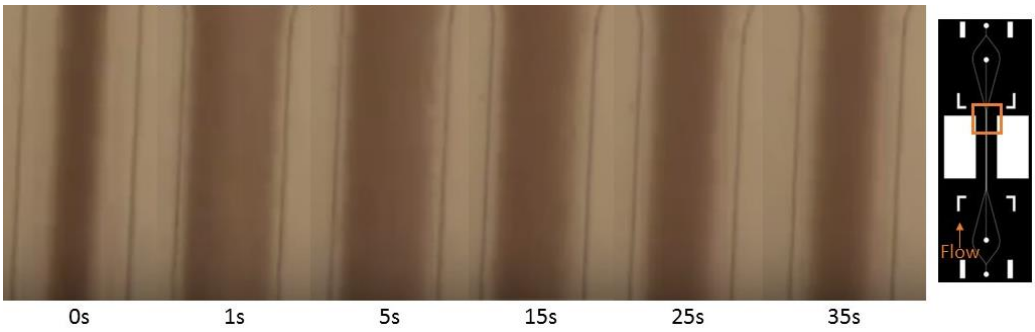

Fig. 41 Changes in the heating of the SSAW transducer were seen to effect transducer performance. Over the course of 30 seconds, the temperature increased by 10°C resulting in the sorting effect fading quickly. This was seen by a reduction in the width of the sample stream following nodal migration at 1 second. The rate of heating was beyond that regulated previously by the temperature regulation system. Changes in blood separation performance within the experiment are likely due to the temperature-dependence of the resonance frequency and transmission properties. The input voltage was 400 mV_{pp}. Flow rates of the sample and buffer were 3 and 10 µL/min, respectively, using the 11Plus pump.

Long-term changes in transducer performance were also observed. Fig. 42 reveals evidence of long-term changes to transducer performance. In the experiment, a voltage of 380 mV_{pp} was applied and flow rates were 3 and 8 µL/min for blood and PBS, respectively, using the 11Plus pump. The sorting effect at low temperature, where high performance blood separation was previously achieved, is relatively weak at 5 and 10 seconds, and is reduced as the device temperature increases several degrees. The maximum transducer temperature measured during

collection of the images in Fig. 42 was 25°C, which previously facilitated significant blood separation. While the rate of heating is low in this experiment, the device does not create high purity separation initially (at several seconds), showing that the performance of the transducer has declined.

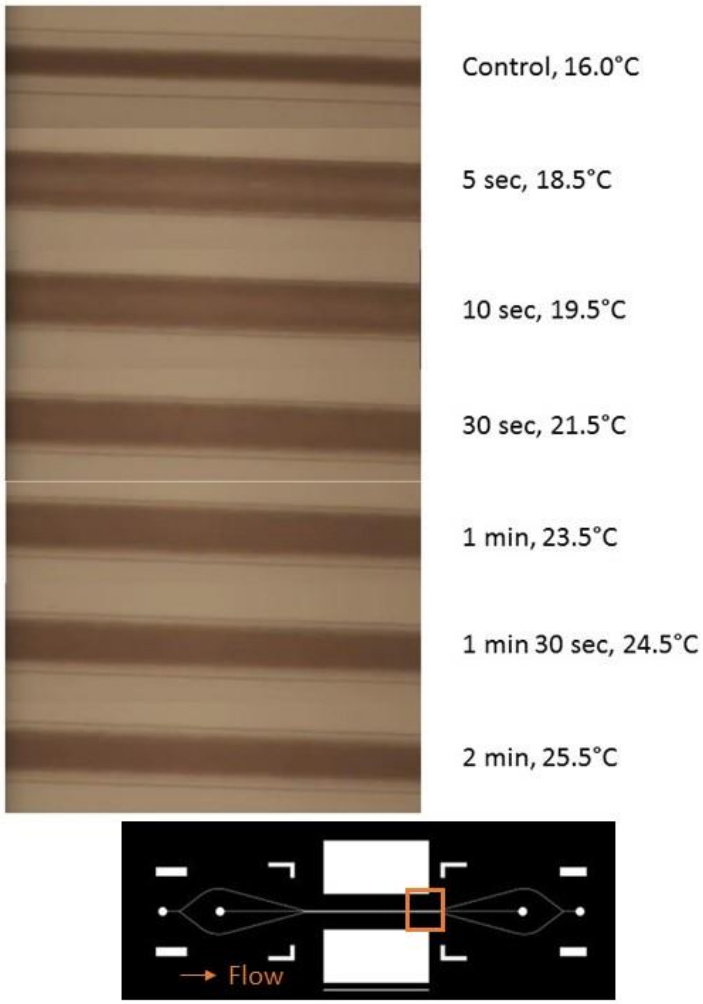

Fig. 42 Long-term changes to transducer performance were observed. The sorting effect at low temperature (~19°C), where high performance blood separation was previously achieved, was seen to be relatively weak at 5 and 10 seconds. The sorting effect was reduced further as the device temperature increases several degrees. The input voltage was 380 mV_{pp}. Flow rates of the sample and buffer were 3 and 8 µL/min, respectively.

In early experiments, it was noted that transducer performance tended to differ slightly from experiment to experiment, requiring a different voltage input for separation or stabilized at a different temperature. However, it is common in radio frequency experiments that performance may depend on changes in the environment. For instance, heating within an experiment may shift the resonance and effect the blood separation performance by reducing transmission when driving the transducer off resonance, as seen in Fig. 41. Therefore, the changes in transducer resonance and transmission properties between experiments, as seen in the transducer results section, were considered normal and the transducer was matched to the new resonance. However, it was also noted that after several weeks of using a particular transducer in experiments that the transducer performance declined, showing either poor ("hazy" or incomplete) blood separation or an inability to be cooled. This degradation of performance over time is believed to be due to changes in the transducer properties. There are a number of potential reasons for these long-term changes in the transducer, including changes in loading, electrode defects, and damage due to over-heating (54, 55). Fig. 43B,C show how some particles, potentially silver from the wire glue, could not be washed off of the electrodes and may have changed the loading and electrical properties of the electrodes compared to Fig. 43A. Scratches to the electrodes may also affect electrode properties and were observed over time. Defects to the electrodes or SAW substrate, like scratches, may have some effect, similar to micro-cracks, or cause changes in wave formation. Over-heating seems a plausible cause for this particular experiment. The amount of "self-heating" in the transducer significantly increases when high frequencies and high voltages are used (54). It could be argued that this experiment uses both high frequency and high voltages. Over-heating can result in micron-scale cracks within the crystal that can shift the resonance and high energy input can cause rearrangement of ions in the

substrate (54-56). Heating may also be changing the properties of the metallic electrode materials, by thermal expansion. Thermal expansion over an experiment is one reason for observing a decrease in power transmission over the course of a "long-term" experiment, as this experiment is. During initial experiments with the transducer, the signal is turned on and off quickly and frequently to test different voltages and other parameters; this could also play into changes in transducer properties. One counter-point is that lithium niobate shows promise for operating in higher temperature environments (56, 57). However, as was seen during fabrication, heating the substrate may exacerbate defects, such as causing existing cracks to propagate. In piezoelectric materials, energy goes into transmission, radiation, conductor loss, and dielectric loss. The amount of energy going into each of these processes may also be changing. The mechanisms of degradation of piezoelectric materials at elevated temperatures are not fully understood (57). It is hypothesized that damage to the electrodes is the most likely reason for changes in transducer performance for this experiment because changes in the electrode surface over time were significant. In addition, the S11 of SSAW transducer #4 was measured directly after fabrication and after months of experiments (with matching circuit removed), and minimal changes were observed. Further investigation would be required to determine the cause definitively.

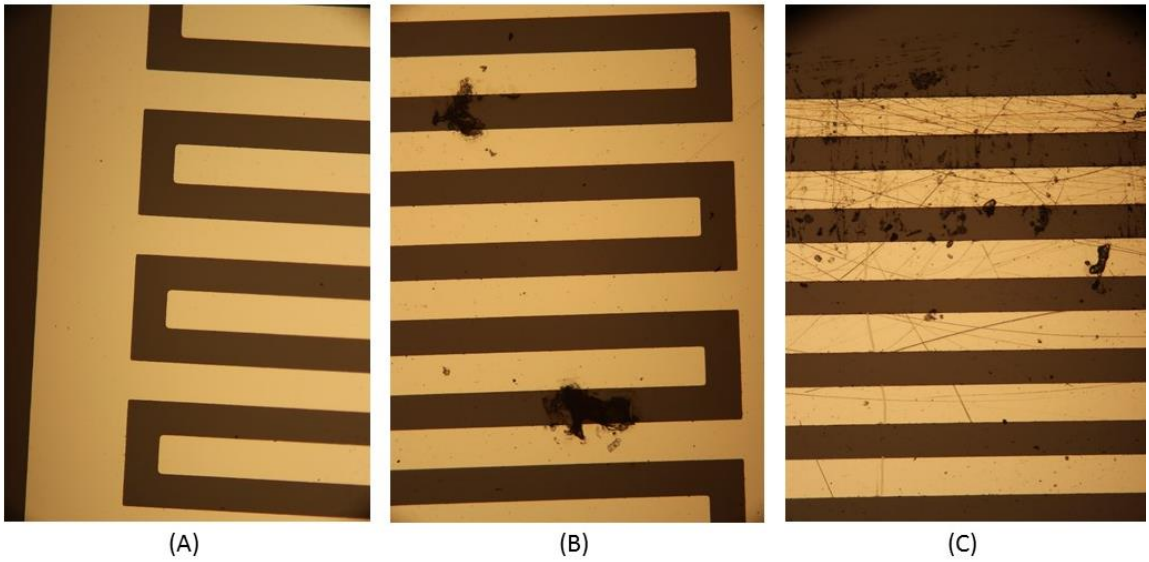

Fig. 43 Debris and scratches left behind from previous experiments may contribute to changes in electrodes performance.

3.5 Effect on Small Particles

Although the transducer performance had decreased, functionalized nanoparticles were added to blood plasma to see if effects from the ARF were observed on the particles. The effect of the flow scenario and acoustic field were observed via the absorption property of the gold nanoparticles, which appear red. Fig. 44 shows the nanoparticle solution in the central stream with PBS sheath fluid in the outer streams at the entrance and exit of the main channel. Flow rates were 3 and 10 μL/min for the nanoparticle-spiked plasma and PBS, respectively. At the exit from the main channel, the nanoparticle stream appears narrower than at the beginning of the channel. This is due to hydro-dynamic focusing of the sample by the sheath fluid. The amount of

diffusion over the 15 mm channel length cannot be determined visually. Some diffusion at the laminar boundaries would be expected.

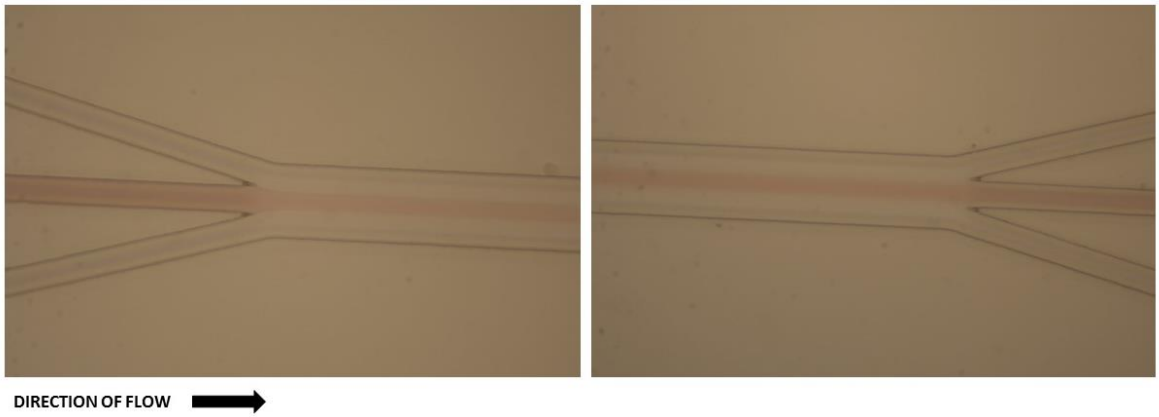

Fig. 44 Laminar streams in a trifurcated microchannel with nanoparticle-spiked plasma located in the sample stream and PBS used as the sheath fluid. At the exit from the main channel (right), the nanoparticle stream appears narrower than at the beginning of the channel (left) due to hydro-dynamic focusing of the sample by the sheath fluid. Diffusion between streams was not obvious. Flow rates were 3 and 10 µL/min for the nanoparticle-spiked plasma and PBS, respectively.

Fig. 45 shows the effect of the SSAW field on the nanoparticle solution for various voltage levels. Prior to this experiment, whole blood was used to align the system. As the voltage is increased, the nanoparticle solution stream widens by greater amounts relative to the control. At 500 mV_{pp}, the nanoparticle solution appears to be dispersed uniformly throughout the channel cross-section. This result indicates that the nanoparticle solution, the suspension fluid, was displaced, as opposed to the nanoparticles, proteins, or other particles contained within the

solution. If the nanoparticles were significantly displaced, the intensity across the channel would not be uniform as the particles move towards the nodal points. According to recent literature, using ARF to manipulate nanoparticles below 200 nm is not efficient (45), even in permanently bonded experiments where power requirements are generally much less than in this work. ASF, on the other hand, can be used to manipulate nanoparticles. Signs of acoustic streaming were not seen in this data. Fluorescent imaging would be a more suitable method to observe ASF contribution. ARF on the fluid medium during acoustophoresis is known to occur when differences in acoustic impedance exist between fluid media. In this case, the acoustic impedance of PBS (Z=1.48 MRayl, (29)) and of blood plasma (Z=1.56 MRayl, (58)) differ; in addition, the relatively high concentration of gold nanoparticles would only increase the density and, therefore, the acoustic impedance of the plasma solution, widening the gap.

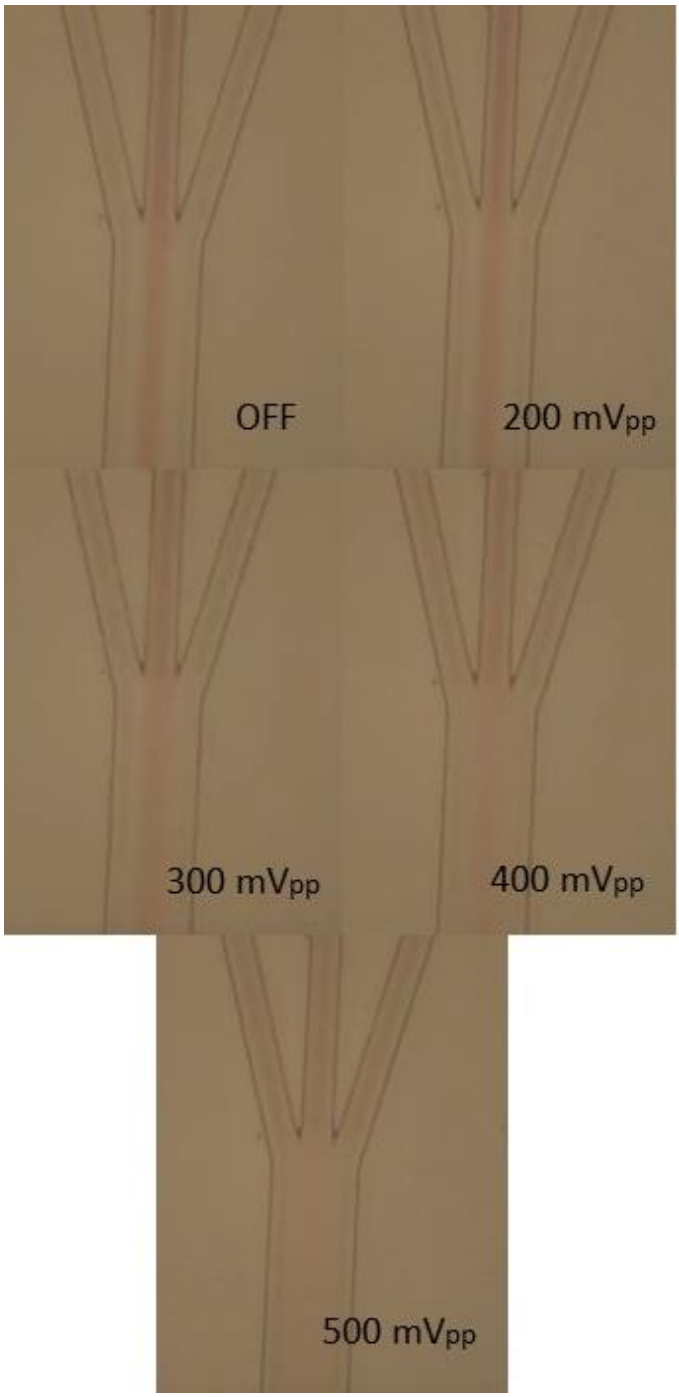

Fig. 45 The effect of the SSAW field on the nanoparticle solution was observed for various voltage levels. As the voltage is increased, the nanoparticle solution stream widens by greater amounts relative to when the transducer is off. At 500 mV_{pp}, the nanoparticle solution appears to be dispersed uniformly throughout the channel cross-section. The ARF appears to have acted on the fluid of the sample as opposed to the particles contained within the solution.

Nanoparticle-plasma solution was allowed to fill the channel and acoustic input was actuated on the stationary sample to observe any changes in color distribution in the channel. No obvious change in absorption distribution was observed (Fig. 46), indicating that nanoparticles were not specifically displaced or driven toward a new location.

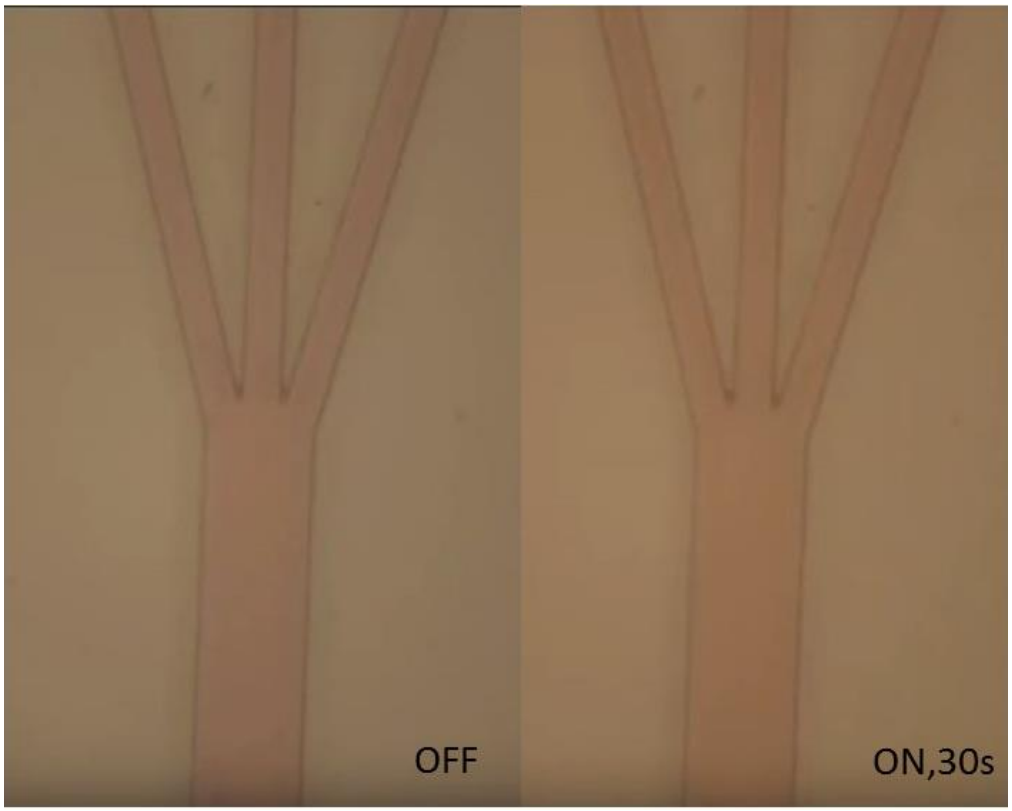

Fig. 46 When nanoparticle solution was allowed to fill the channel, no change in the intensity distribution was observed when the transducer was powered.

The sample was changed to have 10% whole blood content in order to observe any differences between the behavior of the cells, suspension fluid and nanoparticles. Fig. 47 shows the sample flowing through the channel with the transducer off. Apart from a small amount of diffusion, surmised from the "fuzzy" edges of the sample upon exiting the main channel, the fluids remain in their streamlines. It should be noted that two of the branches at the channel exit were clogged, causing all streams to exit the top outlet in the figure below.

Fig. 47 Laminar streams in a trifurcated microchannel with 10% whole blood nanoparticle solution located in the sample stream and PBS used as the sheath fluid. At the exit from the main channel (right), a small amount of diffusion of the sample stream is seen compared with the entrance to the channel (left). Flow rates were 3 and 10 µL/min for the 10% whole blood nanoparticle solution and PBS, respectively.

As in the previous case, dispersion of the sample occurred under the acoustic field. With increasing voltage to the transducer, the sample, both particle (nanoparticle and blood cell) and

suspending fluid, appear to be dispersed throughout the channel cross-section, although blood cells are expected to be preferentially driven toward the nodal positions (Fig. 48). It appears that the ARF on the suspending fluid is greater than the ARF generated on either of the particles of interest, as the blood cells, despite their size, are not seen to specifically migrate toward the nodal positions.

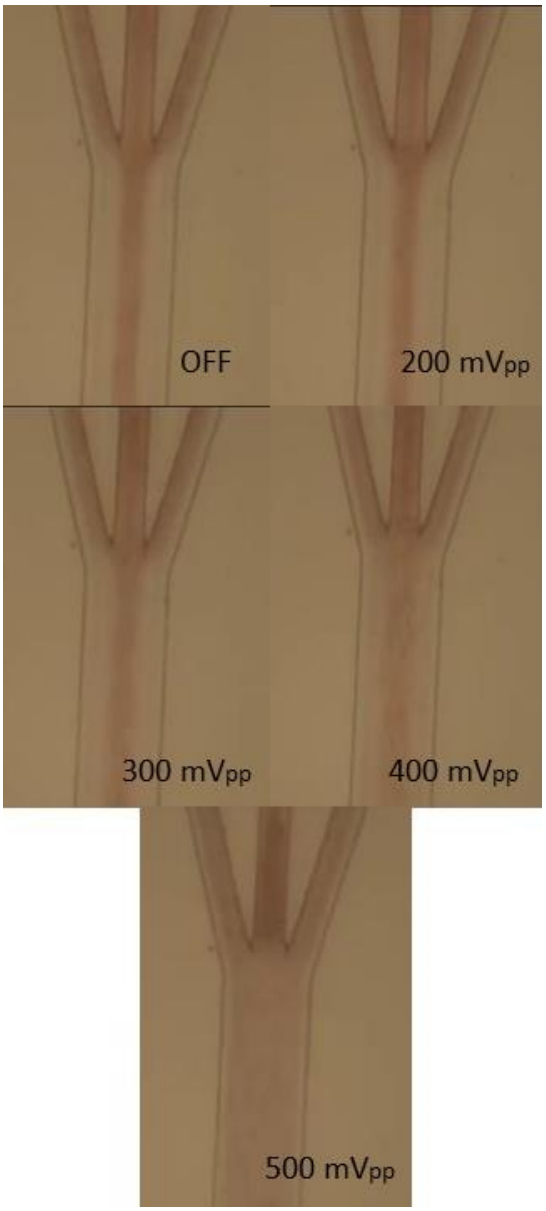

Fig. 48 Effect of SSAW field on 10% whole blood nanoparticle solution for increasing voltage input. With increasing voltage to the transducer, the sample, both particles and suspending fluid, appear to be dispersed throughout the channel cross-section, although blood cells are expected to be preferentially driven toward the nodal positions (Fig. 48). It appears that the ARF on the suspending fluid is greater than the ARF generated on either of the particles of interest, as the blood cells are not seen to specifically migrate toward the nodal positions.

Over the course of this experiment (~two hours), blood sorting per voltage changed. Fig. 49A shows whole blood separation in the channel under 500mV_{pp} acoustic input that was used to confirm channel alignment at the beginning of the experiment. The formation of two nodes is visible at either side of the channel. The second image in the figure (Fig. 49B) shows nanoparticle solution mixed with blood at a 10:1 ratio. In this image, blood cells are dispersed throughout the channel but congregation of particles at nodes is not observed. As the voltage input is the same, this suggests a possible reduction in power transmission or conversion of the transducer over the course of the experiment. Otherwise, with a diluted blood content, displacement of the cells should be similar and higher efficiency than with the whole blood sample used to align the system. This transducer was used for many blood sorting experiments prior to this experiment. However, in previous experiments, although the transducer performance had degraded, such significant changes in blood sorting were not seen within an experiment. Therefore, the separation of blood and nanoparticles using this platform was inconclusive.

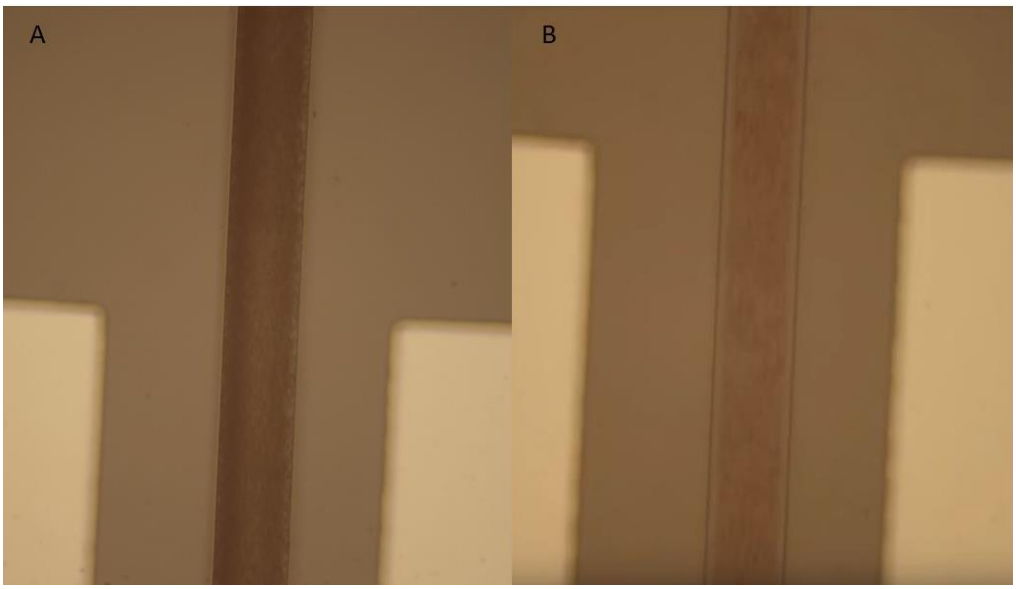

Fig. 49 Blood separation performance was seen to degrade over the course of the experiment. A) Actuating the SSAW transducer at 500 mV_{pp} using whole blood during experiment setup yielded migration of cells to nodal positions. B) Actuating the SSAW transducer at 500 mV_{pp} using 1:10 blood in nanoparticle-doped plasma at the end of the experiment showed no specific organization of cells.

The change in performance may be attributed to changes in the transducer electrodes and substrate as discussed in the blood separation section. However, there are additional possibilities. As the higher acoustic impedance fluid (the sample) is not located at the nodal position, it can be displaced due to the mismatch of acoustic impedance compared with PBS. The speed at which displacement of the sample occurred under acoustic field may indicate that the nanoparticle impedance significantly contributes in this experiment. Considering the properties of gold, the acoustic impedance of the gold nanoparticles would be several times greater than that of blood plasma alone. If this is the case, the displacement of the sample suspension medium may be counteracting or dominating any sorting effects that would normally drive particles to nodal

positions based on size. Diluted blood cells generally require weaker forces to achieve the same level of sorting as whole blood. The lack of blood sorting in this experiment is attributed to both the decay of transducer performance and the mismatch of acoustic impedance between fluids.

CHAPTER IV

CONCLUSION AND FUTURE WORK

The feasibility of an acoustic whole blood separation system using a detachable channel and reusable transducer is explored and nanoparticle distribution under the proposed separation scenario is studied. In this work, several surface acoustic wave transducers were designed and fabricate using chromium and aluminum layers for the electrodes. Resonance frequency of transducers was measured and the devices were matched. Two detachable microfluidic channel designs were fabricated and the displacement of blood cells in both designs was tested with the transducer. The PDMS-PDMS pillar channel design was found to require lower voltage levels for effective particle manipulation. High performance acoustic separation of undiluted whole blood was achieved using the detachable channel and a standing wave format. While the integrated transducer and channel showed potential for blood separation, transducer heating was found to limit long-term blood separation experiments, exceeding several minutes. In order to improve transducer performance, a temperature regulation system was built using a PID loop and Peltier element. The temperature regulation system stabilized the transducer temperature and improved the performance of the transducer for longer experiments. Transducer performance and reuse was found to be limited by changes to transducer properties over time and potential damage. When 15 nm nanoparticle-spiked plasma was used as the sample in the blood separation system, the fluid of the sample was displaced due to its increased acoustic impedance compared with PBS. Separation of whole blood and nanoparticles in this system was inconclusive due to the degradation of the transducer as well as the acoustic impedance mismatch of fluids. One drawback of this system is the apparent increased power requirement for blood sorting due to use

of a temporarily-bonded system. This was expected from previous work on detachable acousto-fluidic systems. Throughout this work, undiluted whole blood separation using a surface acoustic wave transducer and detachable sample cell was seen to be possible. Small particle recovery in the proposed platform requires further investigation.

Future work includes quantification of the blood separation efficiency, nanoparticle recovery and repeatability of the experiment. Studies should be performed to modify the acoustic impedance of the sheath fluid to improve nanoparticle recovery. Biomarker recovery from this system should be studied as well. Optimizing the temperature regulation system may also improve transducer performance. The pressure transmission properties of the microfluidic channel may be explored to reduce power requirements. In addition, future work should focus on the miniaturization of this system for eventual point-of-care applications.

REFERENCES

1. Labcorp, "Results," Labcorp, 7/9/18, https://www.labcorp.com/results#.
2. M. M. L. PLC, "Centrifugation of Blood Specimens," Metropolitan Medical Laboratory PLC, Davenport, Iowa (2018).
3. C. D. Chin, V. Linder, and S. K. Sia, "Lab-on-a-chip devices for global health: Past studies and future opportunities," *Lab on a chip* **7**(1), 41-57 (2007).
4. A. Rios, M. Zougagh, and M. Avila, "Miniaturization through lab-on-a-chip: utopia or reality for routine laboratories? A review," *Analytica chimica acta* **740**(1-11 (2012).
5. P. Abgrall, and A. M. Gué, *Lab-on-chip technologies: Making a microfluidic network and coupling it into a complete microsystem - A review* (2007).
6. R. Pol et al., "Microfluidic lab-on-a-chip platforms for environmental monitoring," *TrAC Trends in Analytical Chemistry* **95**(62-68 (2017).
7. S. Mukherjee et al., "Plasma separation from blood: the 'lab-on-a-chip' approach," *Critical reviews in biomedical engineering* **37**(6), 517-529 (2009).
8. S. F. Green, "The cost of poor blood specimen quality and errors in preanalytical processes," *Clinical biochemistry* **46**(13-14), 1175-1179 (2013).
9. M. Robinson et al., "Rapid isolation of blood plasma using a cascaded inertial microfluidic device," *Biomicrofluidics* **11**(2), 024109 (2017).
10. P. Ohlsson et al., "Integrated Acoustic Separation, Enrichment, and Microchip Polymerase Chain Reaction Detection of Bacteria from Blood for Rapid Sepsis Diagnostics," *Analytical chemistry* **88**(19), 9403-9411 (2016).

11. D. Westermann et al., "High-sensitivity assays for troponin in patients with cardiac disease," *Nature reviews. Cardiology* **14**(8), 472-483 (2017).

12. L. Y. Yeo, and J. R. Friend, "Ultrafast microfluidics using surface acoustic waves," *Biomicrofluidics* **3**(1), 012002 (2009).

13. H. Marks et al., "Ferric plasmonic nanoparticles, aptamers, and magnetofluidic chips: toward the development of diagnostic surface-enhanced Raman spectroscopy assays," *J Biomed Opt* **21**(12), 127005 (2016).

14. H. Kearns et al., "SERS Detection of Multiple Antimicrobial-Resistant Pathogens Using Nanosensors," *Analytical chemistry* **89**(23), 12666-12673 (2017).

15. M. Antfolk, and T. Laurell, "Continuous flow microfluidic separation and processing of rare cells and bioparticles found in blood - A review," *Analytica chimica acta* **965**(9-35 (2017).

16. J. Nam et al., "Separation of platelets from whole blood using standing surface acoustic waves in a microchannel," *Lab on a chip* **11**(19), 3361-3364 (2011).

17. H. Bruus, "Acoustofluidics 7: The acoustic radiation force on small particles," *Lab on a chip* **12**(6), 1014-1021 (2012).

18. D. J. Collins et al., "Continuous micro-vortex-based nanoparticle manipulation via focused surface acoustic waves," *Lab on a chip* **17**(1), 91-103 (2017).

19. C. Devendran, I. Gralinski, and A. Neild, "Separation of particles using acoustic streaming and radiation forces in an open microfluidic channel," *Microfluidics and Nanofluidics* **17**(5), 879-890 (2014).

20. H. Bruus, "Acoustofluidics 10: Scaling laws in acoustophoresis," *Lab on a chip* **12**(9), 1578-1586 (2012).

21. X. Ding et al., "Cell separation using tilted-angle standing surface acoustic waves," *Proceedings of the National Academy of Sciences* **111**(36), 12992-12997 (2014).

22. A. Dolatmoradi, and B. El-Zahab, "Thermally-assisted ultrasonic separation of giant vesicles," *Lab on a chip* **16**(18), 3449-3453 (2016).

23. S. Li et al., "Acoustofluidic bacteria separation," *Journal of Micromechanics and Microengineering* **27**(1), 015031 (2017).

24. G. Destgeer et al., "Continuous separation of particles in a PDMS microfluidic channel via travelling surface acoustic waves (TSAW)," *Lab on a chip* **13**(21), 4210-4216 (2013).

25. P. Ohlsson et al., "Acoustic impedance matched buffers enable separation of bacteria from blood cells at high cell concentrations," *Scientific Reports* **8**(1), 9156 (2018).

26. A. Lenshof et al., "Acoustic Whole Blood Plasmapheresis Chip for Prostate Specific Antigen Microarray Diagnostics," *Analytical chemistry* **81**(15), 6030-6037 (2009).

27. P. Ohlsson, K. Petersson, and T. Laurell, "ACOUSTIC SEPARATION OF BACTERIA FROM BLOOD CELLS AT HIGH CELL CONCENTRATIONS ENABLED BY ACOUSTIC IMPEDANCE MATCHED BUFFERS," *18th International Conference on Miniaturized Systems for Chemistry and Life Sciences* (2014).

28. P. Augustsson et al., "Automated and temperature-controlled micro-PIV measurements enabling long-term-stable microchannel acoustophoresis characterization," *Lab on a chip* **11**(24), 4152-4164 (2011).

29. Y. Chen et al., "High-throughput acoustic separation of platelets from whole blood," *Lab on a chip* **16**(18), 3466-3472 (2016).

30. K. Nogo et al., "Ultrasonic separation of a suspension for in situ spectroscopic imaging," *Optical Review* **23**(360-363 (2016).

31. M. Antfolk et al., "A single inlet two-stage acoustophoresis chip enabling tumor cell enrichment from white blood cells," *Lab on a chip* **15**(9), 2102-2109 (2015).

32. O. Jakobsson et al., "Thousand-Fold Volumetric Concentration of Live Cells with a Recirculating Acoustofluidic Device," *Analytical chemistry* **87**(16), 8497-8502 (2015).

33. Y. Wu et al., "Generation of Autologous Platelet-Rich Plasma by the Ultrasonic Standing Waves," *IEEE transactions on bio-medical engineering* **63**(8), 1642-1652 (2016).

34. S. Datta, *Surface acoustic wave devices*, Prentice Hall (1986).

35. Z. Ma, D. J. Collins, and Y. Ai, "Detachable Acoustofluidic System for Particle Separation via a Traveling Surface Acoustic Wave," *Analytical chemistry* **88**(10), 5316-5323 (2016).

36. R. D. O'Rorke et al., "Acousto-microfluidics: Transporting microbubble and microparticle arrays in acoustic traps using surface acoustic waves," *Journal of Applied Physics* **111**(9), 094911 (2012).

37. B. H. Ha et al., "Acoustothermal heating of polydimethylsiloxane microfluidic system," *Sci Rep* **5**(11851 (2015).

38. H. C. Koydemir, and A. Ozcan, "Mobile phones create new opportunities for microbiology research and clinical applications," *Future Microbiology* **12**(8), 641-644 (2017).

39. Y. Bourquin et al., "Integrated immunoassay using tuneable surface acoustic waves and lensfree detection," *Lab on a chip* **11**(16), 2725-2730 (2011).

40. P. Li et al., "Acoustic separation of circulating tumor cells," *Proceedings of the National Academy of Sciences of the United States of America* **112**(16), 4970-4975 (2015).

41. Z. Wang, "Study of High-Throughput Particle Separation Device Based on Standing Surface Acoustic Wave (SSAW) Technology," University of Akron (2012).

42. Y. Ai, C. K. Sanders, and B. L. Marrone, "Separation of Escherichia coli Bacteria from Peripheral Blood Mononuclear Cells Using Standing Surface Acoustic Waves," *Analytical chemistry* **85**(19), 9126-9134 (2013).

43. S. Li et al., "Acoustofluidic Transfer of Inflammatory Cells from Human Sputum Samples," *Analytical chemistry* **88**(11), 5655-5661 (2016).

44. L. Ren et al., "A high-throughput acoustic cell sorter," *Lab on a chip* **15**(19), 3870-3879 (2015).

45. M. Wu et al., "Acoustic Separation of Nanoparticles in Continuous Flow," *Advanced Functional Materials* **27**(14), 1606039 (2017).

46. J. Hu, "Acoustic Micro/Nano Manipulations: An Editorial Review," *International Journal of Radiology* **1**(1), 1-3 (2014).

47. M. Morteza, and F. J. R., "Acoustic Nanofluidics via Room-Temperature Lithium Niobate Bonding: A Platform for Actuation and Manipulation of Nanoconfined Fluids and Particles," *Advanced Functional Materials* **26**(43), 7861-7872 (2016).

48. C. W. Shields, C. D. Reyes, and G. P. López, "Microfluidic Cell Sorting: A Review of the Advances in the Separation of Cells from Debulking to Rare Cell Isolation," *Lab on a chip* **15**(5), 1230-1249 (2015).

49. S. H. A., and K. S., "Microfluidics: Basic issues, applications, and challenges," *AIChE Journal* **47**(6), 1250-1254 (2001).

50. H. A. Stone, A. D. Stroock, and A. Ajdari, "Engineering Flows in Small Devices: Microfluidics Toward a Lab-on-a-Chip," *Annual Review of Fluid Mechanics* **36**(1), 381-411 (2004).

51. X. Lu et al., "Particle manipulations in non-Newtonian microfluidics: A review," *Journal of Colloid and Interface Science* **500**(182-201 (2017).

52. C. Witte et al., "Microfluidic resonant cavities enable acoustophoresis on a disposable superstrate," *Lab on a chip* **14**(21), 4277-4283 (2014).

53. R. J. Shilton et al., "Rapid and Controllable Digital Microfluidic Heating by Surface Acoustic Waves," *Advanced Functional Materials* **25**(37), 5895-5901 (2015).

54. P. Ronkanen et al., "Self heating of piezoelectric actuators: measurement and compensation," *Micro-Nanomechatronics and Human Science, 2004 and The Fourth Symposium Micro-Nanomechatronics for Information-Based Society, 2004.* 313-318 (2004).

55. R. S. Weis, and T. K. Gaylord, *Lithium Niobate: Summary of Physical Properties and Crystal Structure* (1985).

56. P. Pillatsch et al., "Degradation of Piezoelectric Materials for Energy Harvesting Applications," *Journal of Physics: Conference Series* **557**(1), 012129 (2014).

57. H. d. Castilla, P. Bélanger, and R. J. Zednik, "High temperature characterization of piezoelectric lithium niobate using electrochemical impedance spectroscopy resonance method," *Journal of Applied Physics* **122**(24), 244103 (2017).

58. G. G. Krishna, A. A. ALI, and A. Ahmad, "Absorption of ultrasound in human blood," *Le Journal de Physique Colloques* **51**(C2), C2-311-C312-314 (1990).